Hypothesis Testing based Interference Mitigation in mmWave OFDM Radar

Master Thesis

By Laurits Randers

Aalborg University
Mathematics-Technology

This report is written in the typesetting language LaTeX. Experiments and data processing are conducted using Python 3.13. Illustrations are created using the Inkscape or Python 3.13. References are cited using the IEEE method.

Department of Mathematical Sciences
Thomas Manns Vej 23
DK - 9220 Aalborg Øst
http://www.math.aau.dk

AALBORG UNIVERSITY
STUDENT REPORT

Title:
Hypothesis Testing based Interference Mitigation in mmWave OFDM Radar

Theme:
Master Thesis

Project Period:
Spring Semester 2025

Author:
Laurits Randers

Supervisors:
Martin Voigt Vejling
Petar Popovski

Page Numbers: 43

Date of Completion:
May 27, 2025

Abstract:

This thesis investigates interference mitigation in Orthogonal Frequency Division Multiplexing (OFDM) radar systems for the automotive industry operating at millimetre wave frequencies. An OFDM scheme is introduced that could mitigate interference by using only a subset of subcarriers. A channel model is presented, modelling a scenario where a radar senses the environment in the presence of interferers. An algorithm is proposed for sensing in the presence of interference. It uses a hypothesis test to differentiate between Line-of-Sight (LOS) paths from interferers and backscattered signals from targets. A second hypothesis test is then applied to the LOS paths to detect which subcarriers are affected by interference. The range and path gain of the target are then estimated using only the non-interfered subcarriers. Using a priori angle of arrival, the range of the target can be estimated by doing interference mitigation, improving performance by 5-7dB. However, since the algorithm hasn't been implemented as a complete system, it cannot be definitively concluded on the overall improvement of total sensing performance.

Preface

This master's thesis is written by Laurits Randers, studying Mathematics and Technology at the Department of Mathematical Sciences at Aalborg University. The project is written from February 1, 2025, to May 27, 2025.

I would also like to thank my supervisors, Martin Voigt Vejling and Petar Popovski, for their guidance throughout the project period.

Large language models have been used for spelling and grammatical corrections. Specifically, the models used were GPT-4o by OpenAI and Gemini 2.5 by Google.

Aalborg University, May 27, 2025

Laurits Randers
lrande18@student.aau.dk

Contents

1 Introduction

Radar sensing has become a fundamental technology in the automotive industry, enabling advanced driver assistance systems such as adaptive cruise control, collision avoidance, and autonomous driving. Currently, one of its primary applications is adaptive cruise control, which helps drivers by automatically adjusting the vehicle's speed to maintain a safe following distance from the car ahead. Manufacturers have begun to develop and deploy more advanced driver assistance systems, such as collision avoidance and semi-autonomous driving, which enhance road safety. However, this also increases the requirements for radar measurement accuracy and resolution, as it must reliably distinguish closely spaced and small targets, such as cyclists and pedestrians. The reliability of the radar system plays a crucial role in ensuring road safety [24, pp. 59–60][8, p. 1].

When multiple radars attempt to sense using the same spectrum resources, interference can occur. This can lead to ghost targets, which are not present in the real world, and an increased noise floor, which results in decreased sensing performance [38, p. 1]. This problem is amplified as more manufacturers incorporate radar sensing into their vehicles. Therefore, interference should at least be detected and preferably mitigated to ensure reliable sensing performance [24, p. 62]. Furthermore, it cannot be assumed that the vehicles have a communication link that can be used to allocate spectrum resources, as the cars may come from different manufacturers. Furthermore, there is an overhead when establishing a communication link, which can delay the time it takes to perform sensing. This is not desirable in an automotive application, as it slows down the driver assistance system's response time. Hence, adaptive techniques must be developed that can mitigate interference without relying on communication between the radars [21, p. 143].

Two main technologies have been proposed to play a key role in the future of automotive radar: millimetre-wave (mmWave) radar and Orthogonal Frequency-Division Multiplexing (OFDM) waveforms [24, pp. 60–62].

The International Telecommunication Union has allocated the mmWave spectrum band from 77 to 81 GHz for future automotive radar applications [24, p. 60][32, p. 136]. mmWave radar offers several advantages. The smaller wavelength allows for the design of more compact and cost-effective antenna arrays. More spectrum is available at mmWave frequencies, enabling higher bandwidth, resulting in higher resolution and extended range. At mmWave frequencies, the channel between the transmitter and receiver consists of a few dominant multipath components. This makes the channel highly dependent on the geometry of the environment, which is advantageous for sensing applications [37, p. 81]. Additionally, unlike laser- and camera-based systems, mmWave radar is less affected by weather and lighting conditions [11, pp. 845–846] [24, p. 59]. One disadvantage of mmWave is that the path loss is higher due to the shorter wavelength. However, the small wavelength also enables the construction of compact antenna arrays with a large number of elements. These arrays can be used for highly directional beamforming, which helps compensate for the increased path loss [37, p. 81].

Radar operates by transmitting a waveform and analysing the backscattered signal reflected from objects in the environment. The two most common modulation schemes are Frequency-Modulated Continuous Wave (FMCW) and Orthogonal Frequency-Division Multiplexing (OFDM).

FMCW is currently the most commonly used modulation scheme in the automotive industry. It operates by transmitting a signal whose frequency increases linearly over time within each time slot, allowing the radar to measure both the distance and relative velocity of objects. An illustration of the frequency over time of an FMCW waveform can be seen in Figure 1.1a. Due to the simplicity of the waveform, implementation is low-cost, making it the most commonly used modulation scheme in the automotive industry. [24, pp. 67–68].

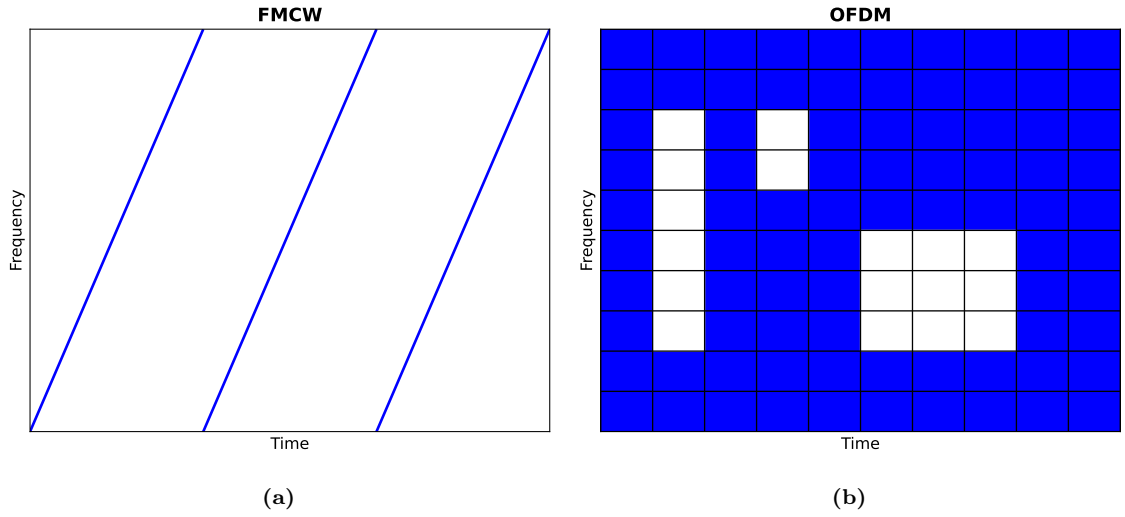

Figure 1.1: Illustration of the frequency over time for **(a)** an FMCW waveform with linear increasing frequency, and **(b)** an OFDM waveform, where not all subcarriers are used simultaneously. The subcarriers used at a given time are highlighted in blue.

Another modulation scheme is OFDM, which was originally used in communication systems. However, it has recently become the focus of significant research in radar systems [4, 19, 14]. In OFDM, multiple symbols are transmitted simultaneously over multiple carrier frequencies, called subcarriers. An illustration of an OFDM waveform over frequency and time can be seen in Figure 1.1b, where the subcarriers used at a given time are highlighted in blue. An advantage of using an OFDM waveform is that it can carry communication data while simultaneously being used for sensing. This concept is known as Integrated Sensing And Communications (ISAC). ISAC is of great interest in the automotive industry, as the communication link can be used by vehicles to share information about their surroundings, road conditions, and potential hazards in real-time, enhancing road safety [7, pp. 23441–23442]. An ISAC waveform can be constructed in three ways: frequency-division, time-division, or fully unified, where sensing and communication share the same time and frequency resources [19, pp. 1743–1744]. If frequency- or time-division is used, the two OFDM waveforms can be designed independently and then combined before transmission [19, p. 1744]. By combining

the sensing and communication waveforms, the same hardware can be used for both tasks, resulting in lower costs and faster development [19, p. 1729] [22, p. 143] [24, pp. 64–65]. OFDM uses a larger amount of bandwidth at a given time. As a result, the likelihood of another radar using the same time-frequency resources increases, which leads to interference [6, pp. 1–2].

However, interference can be mitigated by leveraging the flexibility inherent in OFDM waveforms. In OFDM, a subset of the bandwidth can be used at any given time. This offers a significant advantage for interference mitigation, as the frequencies utilised can change over time. Due to the more flexible waveform and the potential for reusing existing communication hardware, an OFDM waveform will be used for sensing in this thesis.

To use OFDM effectively for sensing, interference mitigation techniques are therefore needed.

Interference mitigation in OFDM radar is analogous to the challenge of multiple access in communication systems, where multiple users transmit simultaneously to a base station. One common solution in communications is Code-Division Multiple Access (CDMA), where each user encodes its signal using an orthogonal code. However, CDMA is not well-suited for radar sensing, as multipath propagation and channel noise can degrade code orthogonality, leading to reduced signal-to-noise ratio (SNR). In sensing applications, significantly higher SNR is required compared to what is acceptable for demodulating digitally encoded signals in communication systems [29, p. 1].

Multiple methods have been proposed for interference mitigation in OFDM radar systems. In the following, a summary of some of the existing solutions for interference mitigation in OFDM radar will be presented.

In [29], a scenario with multiple coordinated OFDM radar transmitters and receivers is considered. To mitigate interference, frequency division was used by assigning sets of subcarriers in an interleaved fashion. This ensures that the transmitters do not interfere with each other. However, this approach assumes that the radars can communicate via a backhaul link to coordinate the subcarriers assigned to each radar.

[22] addresses interference in uncoordinated settings using random subcarrier selection and compressed sensing techniques. It is assumed that the interfered subcarriers have a higher power than the reflected signal and the noise. Those transmitted subcarriers with a power higher than the average are treated as interferences and are not used for sensing. The limited number of subcarriers leads to degraded performance using the conventional sensing algorithms based on the discrete Fourier transform (DFT) methods. To overcome this, a basis pursuit problem from compressed sensing was formulated, which was solved using the YALL1 algorithm. This led to a better output SNR compared to the conventional DFT method.

Similarly, in [33], a method of suppressing narrowband interference in automotive OFDM radar was proposed. This was done by detecting interference in the frequency domain using

atomic norm soft-thresholding from compressed sensing. This led to a better SNR in the range-Doppler space, which led to better sensing performance. This method assumes that the interference is narrowband and not caused by other wideband OFDM users.

In [18], a method for interference mitigation with multiple non-cooperative OFDM radars is proposed. A protocol was developed for multiple OFDM radars to select their subcarriers in a non-cooperative manner to mitigate interference. This proposed method could select nearly optimal subcarriers in a short time with a high probability.

Problem Statement

Current literature detects interference subcarriers by identifying those with power levels higher than a certain threshold. For instance, in [22], the threshold was set as the average power of all subcarriers plus a constant. These approaches have several disadvantages. They do not utilise prior knowledge, such as the beamforming pattern of the transmitter. Furthermore, in threshold-based methods, there is no control over the probability of missed interference detection. This is undesirable, as it may lead to over-detection, where non-interference is falsely classified as interference, resulting in degraded performance. Conversely, interference may also be missed, which likewise leads to degraded system performance.

This can be addressed by applying the theoretical framework of detection theory, which is already widely used in sensing applications to determine whether a target is present or not [34, 28]. Therefore, in this thesis, a method for mitigating interference in OFDM radar using detection theory will be developed. This leads to the following problem statement:

How can a hypothesis test be developed to detect interference in an OFDM mmWave radar system, and can sensing performance be improved by avoiding the use of detected interfered resources?

Scope of Project

In this thesis, a hypothesis test for detecting interference in OFDM radar will be proposed, along with a sensing algorithm that utilises the test. The following assumptions are made in this project: it is assumed that both the targets and the interferers are stationary. This assumption is made to simplify the simulations and modelling, as the main focus of the project is to validate the interference detection. The radars transmit over the same bandwidth using the same OFDM transmission scheme. All radars are assumed to be time-synchronised, meaning that radar transmit symbols start simultaneously. If the symbols are misaligned in time, one symbol may interfere with multiple symbols from another radar. In practice, synchronisation can be achieved using a global navigation satellite system (GNSS) [2]. While this may still result in some desynchronization, it is assumed to be negligible.

Project Outline

The rest of the thesis will be structured as follows: In Chapter 2, the signal model is presented, along with the OFDM scheme used for interference mitigation and the beamformer employed. In Chapter 3, first, an overview of the sensing algorithm is provided. Then, the individual components of the algorithm, together with the corresponding theories, are presented. Numerical results on simulated data are presented in Chapter 4, and the results of the thesis are discussed and concluded in Chapter 5 and Chapter 6, respectively. The potential future work on the project will be discussed in Chapter 7.

2 Signal Model

In this chapter, the signal model used throughout the thesis is presented. First, a short description of the scenarios considered is provided. Then, the OFDM modulation is introduced along with a transmission scheme designed for interference mitigation. Following this, the channel model is described. Finally, the model for the receiver noise and the beamformer used are presented.

The scenario considered in this thesis is as follows. An OFDM radar observes its environment equipped with a Uniform Linear Array (ULA) consisting of N elements, which are used for both transmission and reception. The radar is subject to interference from J interferers, each of which also transmits OFDM signals in the same frequency band as the radar. These interferers are likewise equipped with ULAs of the same size.

Both the radar and the interferers attempt to sense Q targets as well as each other. This leads to interference, as the interferers transmit signals toward the radar, and their signals are also scattered toward the radar after scattering off a target.

The radar and the interferers sense the environment by transmitting OFDM waveforms. In the following section, the OFDM transmission scheme will be presented.

2.1 Orthogonal Frequency-Division Multiplexing

In OFDM, multiple data streams are transmitted simultaneously at different frequencies. An OFDM symbol is transmitted over M different frequencies known as subcarriers, with a spacing of Δf known as the subcarrier spacing, giving a total bandwidth of $W = M\Delta f$. Each symbol is transmitted for a duration of $T = \frac{1}{\Delta f}$, and a total of K symbols are transmitted [14, p. 1395].

The complex baseband signal for the $k \in \{0, 1, \ldots, K-1\}$ symbol transmitted by the radar or interferer $i \in \{0, 1, \ldots, J\}$ is given by:

$$s_k^{(i)}(t) = \sum_{m=0}^{M-1} x_m^{(i)} e^{j2\pi m\Delta f t} \operatorname{rect}\left(\frac{t - kT}{T}\right).$$

Here, $x_m^{(i)}$ is the complex data symbol transmitted by i on the m-th subcarrier and $\operatorname{rect}(t)$ is the rectangular function that equals 1 for $t \in [0, 1]$ and 0 otherwise. Note that $i = 0$ denotes the radar itself [13, p. 3]. Before transmission, the signal is modulated onto a carrier wave of frequency f_c. The transmitted signal over the N transmitting antennas is then given by

$$\operatorname{Re}\left\{\sum_{k=0}^{K-1} \mathbf{f}_k^{(i)} s_k^{(i)}(t) \mathrm{e}^{j2\pi f_c t}\right\}, \quad t \in [0, KT],$$

where $\mathbf{f}_k^{(i)} \in \mathbb{C}^N$ denotes transmitter beamforming vector for the k-th symbol for the i-th transmitter with $\left\|\mathbf{f}_k^{(i)}\right\| = 1$. A transmission of K symbols is referred to as an OFDM frame. [13, p. 3][16, p. 19]. The radar and the interferer are assumed to use the same precoder.

To mitigate interference, both the interferer and the radar utilise only a subset of the total available subcarriers for sensing within one OFDM frame as proposed in [21]. Consequently, the transmitted symbol is defined as:

$$x_m^{(i)} = \begin{cases} 1 & \text{if } m \in \Omega^{(i)} \\ 0 & \text{otherwise,} \end{cases}$$

where $\Omega^{(i)} \subset \Omega$ are the set of resources used by interferer or radar i, and

$$\Omega = \{m | m \in \{0, \dots, M-1\}\},$$

is the total available resources. It is assumed that there is no communication between the radar and the interferer, so they cannot coordinate which subcarriers to use for each frame. So each transmission frame, both the radar and the interferer randomly select the same number of subcarriers, N_s, at random, i.e $|\Omega^{(i)}| = N_s$.

An illustration of two radars selecting subcarriers is shown in Figure 2.1, where red indicates subcarriers selected by both radars, leading to interference.

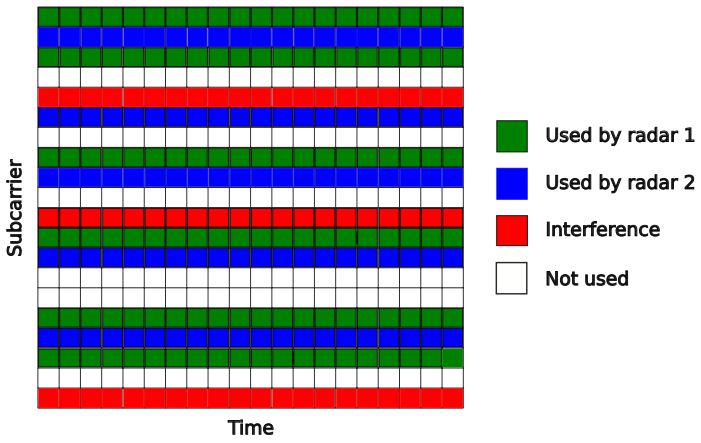

Figure 2.1: A visualisation of the subcarriers used by each radar shows. Interference indicates that a subcarrier is being used by both radars.

Only a subset of the subcarriers is used to minimise the probability of two radars using the same subcarriers. If all radars were to use the entire set of subcarriers and interference occurred, then one or both radars would be unable to sense properly, as all subcarriers would experience interference. As mentioned in the scope of this project, it is assumed that the radar and the interferers are synchronised, such that the states of the one OFDM frame are consistent. This means it can be assumed that the subcarriers used by the radar and the interferers do not change within an OFDM frame.

Next, a channel model is presented for the received signal at the radar.

2.2 Channel Model

At mmWave frequencies, the propagation paths are closely related to the geometry of the environment [35, p. 2817]. Therefore, a geometric-based approach is chosen to model the channel. An illustration of the different signal paths, considering two interferers and one target, is shown in Figure 2.2.

Four types of propagation paths are considered in the model, which are illustrated by different coloured arrows in Figure 2.2: backscatter from the targets (black arrows), backscatter from the interferers (green arrows), LOS paths from the interferers to the radar (blue arrows), and interference signals scattered off the targets to the radar (red arrows).

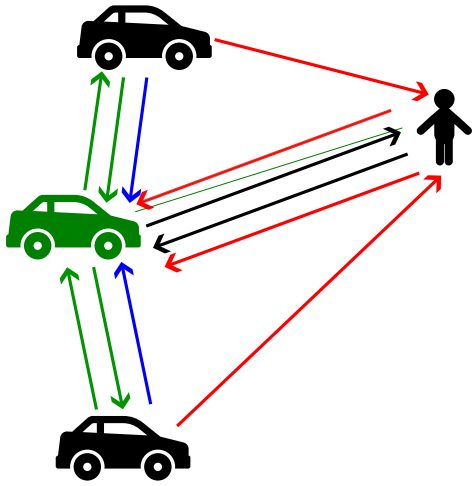

Figure 2.2: Illustration of the signal paths in the scenario. The radar is represented by the green car, the interferers by the black cars, and the target by the person. Coloured arrows indicate different signal paths: black arrows represent the backscatter signals from the target, green arrows denote backscatter from the interferers, blue arrows indicate the LOS paths travelling directly from the interferers to the radar, and red arrows depict interference signals that are scattered off the target.

Using this, the channel model of the received signal at the radar can be stated. The received signal at the radar in the frequency domain at the N receive antennas for subcarrier $m \in \{0, 1 \ldots, M-1\}$ and symbol $k \in \{0, 1 \ldots, K-1\}$ is given by

$$\mathbf{y}_{k,m} = \sum_{l=0}^{Q+J-1} \mathbf{H}_{k,m}^{\text{sctr},l} \mathbf{f}_k^{(0)} x_m^{(0)} + \sum_{j=1}^{J} \mathbf{H}_{k,m}^{\text{int},j} \mathbf{f}_k^{(j)} x_m^{(j)} + \mathbf{n}_{k,m}.$$

Here, $\mathbf{y}_{k,m} \in \mathbb{C}^N$ represents the received signal in the frequency domain, and $\mathbf{n}_{k,m} \sim \mathcal{CN}(\mathbf{0}, \sigma^2 \mathbf{I}_N)$ is circularly symmetric complex additive white Gaussian noise, which is assumed to be independent across frequency and time [34, p. 2][13, p. 3]. The matrix $\mathbf{H}_{k,m}^{\text{sctr},l} \in \mathbb{C}^{N \times N}$ represents the radar's backscatter, which ideally would be used for sensing. It consists of backscatter of the Q targets and the J interferers, as illustrated by the black and green arrows in Figure 2.2.

Finally, $\mathbf{H}_{k,m}^{\text{int},j} \in \mathbb{C}^{N\times N}$ represents the channel matrix of the interference signal from the j-th interferer to the radar. The interference consists of the LOS path and the backscatter of the target, illustrated by the blue and red arrows, respectively, in Figure 2.2. [35, p. 2817] [13, p. 3]. Note that, depending on the scenario, not all paths may be present.

$\mathbf{H}_{k,m}^{\text{sctr},l}$ represents the channel between the radar and a scatterer that the radar is trying to sense, which is either an interferer or a target. The channel matrix for a path reflected by a scatterer is given by [35, p. 2817]:

$$\mathbf{H}_{k,m}^{\text{sctr},l} = \alpha^{\text{sctr},l}\mathbf{a}_{\text{rx}}(\theta^{\text{sctr},l})\mathbf{a}_{\text{tx}}^{\top}(\phi^{\text{sctr},l})\mathrm{e}^{-j2\pi m\Delta f\tau^{\text{sctr},l}},$$

where α is the complex channel gain, θ and ϕ represent the angle of arrival and angle of departure, respectively and τ is the time of arrival of the received signal. $\mathbf{a}_{\text{rx}} \in \mathbb{C}^N$ and $\mathbf{a}_{\text{tx}} \in \mathbb{C}^N$ denote the steering vectors of the receive and transmit antennas, respectively. It is assumed that the same ULA is used for transmission and receiving. The steering vectors of a ULA are given by:

$$\mathbf{a}_{\text{tx}\backslash\text{rx}}(\theta) = \left[1, \mathrm{e}^{-j2\pi\frac{d}{\lambda}\sin(\theta)}, \mathrm{e}^{-j4\pi\frac{d}{\lambda}\sin(\theta)}, \ldots, \mathrm{e}^{-j2\pi\frac{d}{\lambda}\sin(\theta)(N-1)}\right]^{\top},$$

where d is the antenna spacing and $\lambda = \frac{c}{f_c}$ is the wavelength of the carrier with c denoting the speed of light. In this project, the antenna spacing $d = \frac{\lambda}{2}$ is used, as this provides the highest spatial resolution [14, p. 3].

The complex channel gain for all the paths is given by

$$\alpha = |\alpha|\,\mathrm{e}^{j\vartheta},$$

where phase is independent uniformly disubstituted from $[0, 2\pi)$ i.e $\vartheta \sim \mathcal{U}[0, 2\pi)$ [15, p. 1887]. The amplitude depends on the type of path.

For a scatter path of the l-th scatterer the amplitude is given by [1, p. 4947]

$$\left|\alpha^{\text{sctr},l}\right|^2 = \frac{E_s^{(0)}\lambda^2\sigma_{\text{RCS}}^{(l)}}{(4\pi)^3\left\|\mathbf{p}_{\text{s}}^{(l)}\right\|^4}, \tag{2.1}$$

where $\mathbf{p}_{\text{s}}^{(l)} = [p_{\text{s,x}}^{(l)}, p_{\text{s,y}}^{(l)}]^{\top}$ is the position vector of the l-th scatterer, $\sigma_{\text{RCS}}^{(l)}$ is the radar cross-section of the scatterer, λ is the wavelength of the carrier and $E_s^{(0)}$ is the transmitted energy per symbol of the radar. The coordinate system is defined with the radar positioned at the origin.

For the scatter paths the time-of-arrival, angle-of-arrival and angle-of-departure are given by

$$\tau^{\text{sctr},l} = \frac{2\left\|\mathbf{p}_{\text{s}}^{(l)}\right\|}{c},$$
$$\phi^{\text{sctr},l} = \theta^{\text{sctr},l} = \arctan2(p_{\text{s,y}}^{(l)}, p_{\text{s,x}}^{(l)}),$$

where $\arctan2(y, x)$ is the angle between the x-axis and the vector $[x, y]^\top$ and c is the speed of light. The radio wave is reflected straight back at the radar, hence $\phi^{\text{sctr},l} = \theta^{\text{sctr},l}$ [15, p. 1888].

The interference channel matrix $\mathbf{H}_{k,m}^{\text{int},j}$ from the j-th interferer can be decomposed into a line-of-sight component and a reflection of the target, represented by the blue and red arrows on Figure 2.2, respectively. Thus, the interference channel matrix is given by:

$$\mathbf{H}_{k,m}^{\text{int},j} = \mathbf{H}_{k,m}^{\text{LOS},j} + \sum_{q=0}^{Q-1} \mathbf{H}_{k,m}^{\text{refl},j,q}.$$

The line-of-sight path is represented in the same manner as the scattered paths.

$$\mathbf{H}_{k,m}^{\text{LOS},j} = \alpha^{\text{LOS},j} \mathbf{a}_{\text{rx}}(\theta^{\text{LOS},j}) \mathbf{a}_{\text{tx}}^\top(\phi^{\text{LOS},j}) \mathrm{e}^{-j2\pi m \Delta f \tau^{\text{LOS},j}},$$

The amplitude of the channel gain for the line-of-sight path is given by [35, p. 2817]:

$$\left|\bar{\alpha}^{\text{LOS},j}\right|^2 = \frac{E_s^{(j)} \lambda^2}{(4\pi)^2 \left\|\mathbf{p}_{\text{int}}^{(j)}\right\|^2},$$

where $\mathbf{p}_{\text{int}}^{(j)} = [p_{\text{int,x}}^{(j)}, p_{\text{int,y}}^{(j)}]$ is the position vector of the j-th interferer and $E_s^{(j)}$ is the transmitted energy per symbol by the j-th interferer. The time-of-arrival, angle-of-arrival and angle-of-departure are given by

$$\begin{aligned}
\tau^{\text{LOS},j} &= \frac{\left\|\mathbf{p}_{\text{int}}^{(j)}\right\|}{c}, \\
\theta^{\text{LOS},j} &= \arctan2(p_{\text{int,y}}^{(j)}, p_{\text{int,x}}^{(j)}), \\
\phi^{\text{LOS},j} &= \theta^{\text{LOS},j} - \pi.
\end{aligned}$$

For simplicity, it is assumed that the antenna arrays of the interferers have the same orientation as the receiver; hence, $\phi^{\text{LOS},j} = \theta^{\text{LOS},j} - \pi$.

The final component of the interference channel consists of interference signals scattered by the target towards the radar. The path of the signal from the j-th interferer, after being scattered off the q-th target is given by

$$\mathbf{H}_{k,m}^{\text{refl},j,q} = \alpha^{\text{refl},j,q} \mathbf{a}_{\text{rx}}(\theta^{\text{refl},j,q}) \mathbf{a}_{\text{tx}}^\top(\phi^{\text{refl},j,q}) \mathrm{e}^{-j2\pi m \Delta f \tau^{\text{refl},j,q}}.$$

The amplitude of the path gain is determined in the same manner as for the scattered path (2.1) :

$$\left|\alpha^{\text{refl},j,q}\right|^2 = \frac{E_s^{(j)} \lambda^2 \sigma_{\text{RCS}}^{(q)}}{(4\pi)^3 \left\|\mathbf{p}_{\text{s}}^{(q)} - \mathbf{p}_{\text{int}}^{(j)}\right\|^2 \left\|\mathbf{p}_{\text{s}}^{(q)}\right\|^2},$$

where $\sigma_{\text{RCS}}^{(q)}$ is the radar cross-section of the q-th target [1, p. 4947].

The corresponding time-of-arrival, angle-of-arrival and angle-of-departure are given by

$$\begin{aligned}\tau^{\text{refl},j,q} &= \frac{\left\|\mathbf{p}_{\text{s}}^{(q)} - \mathbf{p}_{\text{int}}^{(j)}\right\| + \left\|\mathbf{p}_{\text{s}}^{(q)}\right\|}{c},\\ \phi^{\text{refl},j,q} &= \arctan2(p_{s,y}^{(q)} - p_{\text{int,y}}^{(j)}, p_{s,x}^{(q)} - p_{\text{int,x}}^{(j)}),\\ \theta^{\text{refl},j,q} &= \arctan2(p_{s,y}^{(q)}, p_{s,x}^{(q)}).\end{aligned}$$

Lastly, the model used for the receiver noise and the beamforming used are presented.

2.3 Receiver Noise

When receiving radar signals, the received signal contains noise. This noise may stem from the receiver's amplifier and external sources such as other transmitters. However, even in an environment with no external noise sources and a noiseless amplifier, the receiver still experiences thermal noise. Thermal noise arises from the random thermal motion of conduction electrons and is always present, regardless of the electrical potential of the conductor [27, p. 33]. Since external noise sources are difficult to model accurately, only thermal noise will be considered in the analysis.

The power spectral density (PSD) of the thermal noise is constant and is given by:

$$N_0 = k_B T_{\text{room}},$$

where $k_B = 1.38 \cdot 10^{-23} \frac{\text{J}}{\text{K}}$ is the Boltzmann's constant and $T_{\text{room}} = 295\text{K}$ is room temperature (22C°) in Kelvin [27, p. 33]. Using this, the variance of the noise per subcarrier can be calculated as [27, p. 33]:

$$\sigma^2 = N_0 \Delta f.$$

2.4 Beamforming Design

The radar and the interferer are both using the same transmit beamforming vectors $\mathbf{f}_k^{(i)}$. For each OFDM symbol, the radar transmits one beam. The transmission is designed such that within one OFDM frame, the angular interval $\left[-\frac{\pi}{2}, \frac{\pi}{2}\right]$ is swept.

The transmit beamforming vector at OFDM symbol k for the ith radar is given by [1, p. 4941]:

$$\mathbf{f}_k^{(i)} = \frac{1}{N}\mathbf{a}_{\text{tx}}^*(\phi_k).$$

At the kth OFDM symbol, a single beam is transmitted in the direction of ϕ_k. The angles ϕ_k are chosen to be uniformly spaced over the interval $\left[-\frac{\pi}{2}, \frac{\pi}{2}\right]$, and are given by:

$$\phi_k = -\frac{\pi}{2} + \frac{k\pi}{K-1}, \quad k \in \{0, \ldots, K-1\}.$$

The transmitted power in the direction of θ is given by:

$$P_{\text{tx}}(\theta) = \mathbf{a}_{\text{tx}}^H(\theta)\mathbf{R}_\mathbf{f}\mathbf{a}_{\text{tx}}(\theta),$$

where $\mathbf{R}_\mathbf{f}$ is the autocorrelation matrix of the precoder signal, given by [17, p. 72]:

$$\mathbf{R}_\mathbf{f} = \sum_{k=0}^{K-1} \mathbf{f}_k^H \mathbf{f}_k.$$

The power is normalised before plotting, so the normalised transmitted power is defined as:

$$P_{\text{tx}}(\theta) = \frac{P_{\text{tx}}(\theta)}{P_{\max}},$$

where $P_{\max} = \max_\theta P_{\text{tx}}(\theta)$ [17, p. 72].

3 Proposed Algorithm

In this chapter, the proposed algorithm for sensing in the presence of interference is presented. The goal is to estimate the time of arrival $\tau^{(d)}$, the angle of arrival $\theta^{(d)}$ and the channel gain $\alpha^{(d)}$ of the targets and the interferers, which can then be used to estimate their locations while the radar experiences interference.

To mitigate interference, the radar needs to estimate the subcarriers used by the interferers. The strongest path to an interferer is typically the Line-of-Sight (LOS) path, if present [37, p. 83]. For this reason, the LOS path is used to detect which subcarriers the interferers are occupying. The rationale for using the LOS path is that interference from the backscatter of targets can be challenging to distinguish from the radar's own backscatter signal, especially since they can have similar power levels if they are at the same distance from the target.

To determine which paths are LOS, the number of unique paths D is first estimated, along with their corresponding angles of arrival (AOA) $\hat{\theta}^{(d)}$. Then, a hypothesis test is applied to each AOA to determine which of them corresponds to a LOS path. This is achieved by setting an upper bound on how strong the channel gain of a hypothetical target path can be. If a given path's channel gain is higher than expected for a hypothetical target, it is classified as an LOS path.

If the LOS path has a lower channel gain than the threshold, the interferer is assumed to be far enough away that it does not significantly affect the sensing performance.

The paths classified as LOS (if any) are used to estimate the subcarriers utilised by the interferer. Note that there may be more than one interferer.

This is done by performing another hypothesis test on each LOS path for each of the subcarriers used by the radar. The test follows the same principle as the first, but the channel gain is only estimated using a single subcarrier at a time. If the estimated channel gain on that subcarrier exceeds the threshold, it is classified as interfered. The set of all interfered subcarriers is denoted $\Omega^{(i)}$. Hence, the set of non-interfered subcarriers can be calculated as $\Omega^{(s)} = \Omega^{(0)} \setminus \Omega^{(i)}$. The reason for first identifying which AOAs correspond to LOS interferers before testing the individual subcarriers is to limit the total number of hypothesis tests. This is done to reduce computational complexity and lower the probability of falsely classifying non-interfered subcarriers as interfered.

Then, for each path, the time of arrival $\hat{\tau}^{(d)}$ and the channel gain $\hat{\alpha}^{(d)}$ are estimated using only the non-interfered resources $\Omega^{(s)}$. This is also done for the LOS paths, as the channel may experience backscatter from the interferer, which can be used to estimate the position of the interferer.

The proposal is summarised in Algorithm 1.

Algorithm 1 Proposed Algorithm

1. Estimate the number of paths D and the AOAs $\{\hat{\theta}^{(d)}\}_{d=0}^{D-1}$ for the paths.
2. Determine whether each path is a LOS path or a backscatter path.
3. Estimate the interference resources $\Omega^{(i)}$ using the LOS paths.
4. Estimate the remaining parameters of each path $\{\hat{\tau}^{(d)}, \hat{\alpha}^{(d)}\}_{d=0}^{D-1}$ using the non-interfered resources $\Omega^{(s)} = \Omega^{(0)} \setminus \Omega^{(i)}$.

The steps in Algorithm 1 will be elaborated in the following sections. In Section 3.1, an algorithm based on MUSIC will be presented to determine the number of paths D and the AOAs $\{\hat{\theta}^{(d)}\}_{d=0}^{D-1}$. In Section 3.2, a hypothesis test will be derived to identify which AOAs correspond to LOS paths. In Section 3.3, another hypothesis test will be presented that uses the LOS paths to identify which subcarriers are used by the interferers. Lastly, in Section 3.4, a method for estimating the time of arrival and, consequently, the range of the targets and interferers using only the non-interfered subcarriers will be derived.

3.1 Angle of Arrival Estimation

Before determining whether interference is present and which resources the interferer is using, the AOAs of the individual paths must first be estimated.

Multiple algorithms exist for AOA estimation, such as the Maximum Likelihood Estimate (MLE). However, MLE is computationally expensive, especially when multiple sources are present [25, p. 279]. A less computationally demanding method is conventional (or Bartlett) beamforming, which computes the correlation between the spatial covariance matrix and the steering vector of the antenna array. However, this method suffers from poor resolution and cannot distinguish closely spaced sources compared to other techniques [25]. The Capon method, also known as Minimum Variance Distortionless Response (MVDR) beamforming, offers improved ability to distinguish between closely spaced targets compared to classical methods [5]. For even finer resolution, especially with targets that are very close, the MUltiple SIgnal Classification (MUSIC) algorithm [25] is often preferred and will be employed in the proposed method.

Assume that there are L propagation paths arriving at the receiving antenna. These paths can include backscatter from the target, backscatter from the interferer, LOS interference, or interference signals reflected off the targets. Some of these paths may share the same AOA. For instance, the backscatter from the interferer and the LOS path from that interferer may have the same or very similar AOAs. Thus, interference can be used as an advantage in the case of these AOAs, as it increases their power.

For ease of notation, the received signal in the frequency domain at subcarrier m and OFDM symbol k is denoted as the sum of the L paths:

$$\mathbf{y}_{k,m} = \sum_{l=0}^{L-1} \alpha^{(l)} \mathbf{a}_{\text{rx}}(\theta^{(l)}) \mathbf{a}_{\text{tx}}^{\top}(\phi^{(l)}) \mathrm{e}^{-j2\pi m \Delta f \tau^{(l)}} \mathbf{f}_k^{(l)} x_m^{(l)} + \mathbf{n}_{k,m}.$$

Note that some of the values may be the same for different paths for instance, terms like $\mathbf{f}_k^{(l)} x_m^{(l)}$ may be identical when the signal is transmitted from the same source (either the radar it self or an interferer), and AOAs $\theta^{(l)}$ may also coincide as noted earlier. This means that there are at most L distinct AOAs arriving at the receiver. The number of unique AOAs will be denoted as $D \leq L$.

The MUSIC algorithm operates on the principle that the signal and noise components are statistically independent. This implies that the received signal can be decomposed into a signal subspace and a noise subspace, which are orthogonal to each other [25, pp. 276–277]. The noise and signal subspaces are separated by performing eigenvalue decomposition of the spatial covariance matrix.

First, a theoretical expression for the spatial covariance matrix will be derived using the methodology presented in [14, Lemma 1][1]. The spatial covariance of the received signal is given by

$$\mathbf{R} = \mathbb{E}\left[\sum_{k=0}^{K-1}\sum_{m=0}^{M-1} \mathbf{y}_{k,m}^H \mathbf{y}_{k,m}\right] = \mathbf{R}^{\text{direct}} + \mathbf{R}^{\text{cross}} + KM\sigma^2\mathbf{I}_N.$$

$\mathbf{R}^{\text{direct}}$ represents the direct terms corresponding to the correlation of each path with itself, while $\mathbf{R}^{\text{cross}}$ contains the cross terms representing the correlations between different paths. The expected values of the signal-noise cross terms are zero, as it is assumed that the transmitted signal and the noise are uncorrelated. The last term originates from the noise component and is given by:

$$\mathbb{E}\left[\sum_{k=0}^{K-1}\sum_{m=0}^{M-1} \mathbf{n}_{k,m}^H \mathbf{n}_{k,m}\right] = KM\sigma^2\mathbf{I}_N.$$

The direct terms are given by

$$\mathbf{R}^{\text{direct}} = \sum_{k=0}^{K-1}\sum_{m=0}^{M-1}\sum_{L=0}^{L-1} |\alpha^{(l)}\mathbf{a}_{\text{tx}}^\top(\phi^{(l)})\mathbf{f}_k^{(l)}|^2 |x_m|^2 \mathbf{a}_{\text{rx}}^H(\theta^{(l)})\mathbf{a}_{\text{rx}}(\theta^{(l)})$$

By using that $|x_m|^2 = 1$ and letting $\beta^{(l)} = |\alpha^{(l)}|^2 \sum_{k=0}^{K-1} |\mathbf{a}_{\text{tx}}^\top(\phi^{(l)})\mathbf{f}_k^{(l)}|^2$

$$\mathbf{R}^{\text{direct}} = M\sum_{L=0}^{L-1} \beta^{(l)}\mathbf{a}_{\text{rx}}^H(\theta^{(l)})\mathbf{a}_{\text{rx}}(\theta^{(l)}).$$

If it is assumed that the paths are sufficiently separated in time of arrival and angle of arrival, it can be assumed that the cross-correlations are negligible, i.e., $\mathbf{R}^{\text{cross}} \approx \mathbf{0}_{N\times N}$, where $\mathbf{0}_{N\times N}$ is the $N \times N$ zero matrix [14, Lemma 1].

Hence, theoretically, the spatial covariance matrix is given by:

$$\begin{aligned}\mathbf{R} &\approx \mathbf{R}^{\text{direct}} + KM\sigma^2\mathbf{I}_N \\ &= M\sum_{L=0}^{L-1} \beta^{(l)}\mathbf{a}_{\text{rx}}^H(\theta^{(l)})\mathbf{a}_{\text{rx}}(\theta^{(l)}) + KM\sigma^2\mathbf{I}_N.\end{aligned}$$

[1] Most of the derivation is provided in the supplementary material, which is available on arXiv.

It is observed that $\mathbf{R}^{\text{direct}}$ is a rank-D matrix, provided that $N > D$ [25, p. 277], [14, p. 1397]. Note that the rank of $\mathbf{R}^{\text{direct}}$ depends on the number of unique AOAs D, not the total number of paths L. By this, the eigenvalue decomposition of the spatial covariance matrix is given by

$$\mathbf{R} = \mathbf{U}_s \mathbf{\Lambda}_s \mathbf{U}_s + \mathbf{U}_n \mathbf{\Lambda}_n \mathbf{U}_n.$$

Where $\mathbf{\Lambda}_s$ is a diagonal matrix containing the D largest eigenvalues, and $\mathbf{U}_s$ contains the corresponding eigenvectors which span the signal subspace. $\mathbf{\Lambda}_n$ contains the remaining $N-D$ smaller eigenvalues, which are all equal to $KM\sigma^2$, and $\mathbf{U}_n$ contains their corresponding eigenvectors which span the noise subspace [25, p. 277].

It can be seen from (3.1) that the received signal with AOA θ_l is correlated with the receive steering vector in that direction, $\mathbf{a}_{\text{rx}}(\theta_l)$ [25, p. 277].

Hence, per the assumption that the signal is uncorrelated with the noise $\mathbf{U}_n^H \mathbf{a}_{\text{rx}}(\theta^{(l)}) = \mathbf{0}$ and so

$$\left\| \mathbf{U}_n^H \mathbf{a}_{\text{rx}}(\theta^{(l)}) \right\|^2 = \mathbf{a}_{\text{rx}}^H(\theta^{(l)}) \mathbf{U}_n \mathbf{U}_n^H \mathbf{a}_{\text{rx}}(\theta^{(l)}) = 0. \tag{3.1}$$

This will be used to estimate the AOAs using an estimate of the noise subspace. This is done by first estimating the spatial covariance matrix by averaging over all frequency and time samples [14, p. 1397]:

$$\hat{\mathbf{R}} = \sum_{k=0}^{K-1} \sum_{m=0}^{M-1} \mathbf{y}_{k,m}^H \mathbf{y}_{k,m} \in \mathbb{C}^{N \times N}.$$

Then taking the eigenvalue decomposition of the estimated spatial covariance matrix $\hat{\mathbf{R}}$

$$\hat{\mathbf{R}} = \hat{\mathbf{U}}_s \hat{\mathbf{\Lambda}}_s \hat{\mathbf{U}}_s + \hat{\mathbf{U}}_n \hat{\mathbf{\Lambda}}_n \hat{\mathbf{U}}_n.$$

Where $\hat{\mathbf{\Lambda}}_s$ is a diagonal matrix containing the $\hat{D}$ largest eigenvalues, and $\hat{\mathbf{U}}_s$ contains the corresponding eigenvectors which estimate the signal subspace. $\hat{\mathbf{\Lambda}}_n$ contains the remaining $N - \hat{D}$ smaller eigenvalues, and $\hat{\mathbf{U}}_n$ contains their corresponding eigenvectors that estimated the noise subspace [25, p. 277]. The estimate of the dimension of the signal space, $\hat{D}$, can be found by sorting the eigenvalues of $\hat{\mathbf{R}}$ and calculating the difference between consecutive eigenvalues. The index corresponding to the first difference that is larger than a given threshold is taken as $\hat{D}$. However, in this thesis, the number of sources is assumed to be known a priori.

By taking the reciprocal of (3.1), using the estimated noise eigenvectors $\hat{\mathbf{U}}_s$, the MUSIC spectrum is constructed, which exhibits peaks at the AOAs

$$P_{\text{MUSIC}}(\theta) = \frac{1}{\mathbf{a}_{\text{rx}}^H(\theta) \hat{\mathbf{U}}_n \hat{\mathbf{U}}_n^H \mathbf{a}_{\text{rx}}(\theta)}.$$

The AOAs can be estimated by finding the $\hat{D}$ peaks in the MUSIC spectrum [25, p. 278].

3.2 Line-of-Sight Detection

This section provides a method for identifying which AOAs originate from LOS paths. To identify the LOS paths, the following hypothesis test is used:

$$H^0 : \text{Non LOS interference path}$$
$$H^1 : \text{LOS interference path.}$$

The null hypothesis H^0 represents the case where a path consists only of noise, backscatter from a target, or both. The alternative hypothesis H^1 represents the case where the path is a LOS path to an interferer. In the following, a test statistic will be derived, similar to what was proposed in [34]. To derive the test statistic, it is assumed that under the null hypothesis, the strongest possible target is present. This assumption is made because it is the worst-case scenario. The test statistic is derived to determine whether the path gain is higher than that of the strongest possible target. If the path gain is higher than the strongest possible target, it must be a LOS path.

It is assumed that the angle of arrival of the path $\hat{\theta}$ is already estimated. The hypothetical received signal from the path corresponding to a backscatter from a target without interference is given by:

$$\tilde{\mathbf{y}}_{k,m} = \tilde{\alpha}\mathbf{a}_{\text{rx}}(\hat{\theta})\mathbf{a}_{\text{tx}}^{\top}(\hat{\theta})\mathbf{f}_k^{(0)}x_m^{(0)}\mathrm{e}^{-j2\pi m\Delta_f\tilde{\tau}} + \mathbf{n}_{k,m}$$

where $\tilde{\alpha}$ and $\tilde{\tau}$ are the hypothetical channel gain and angle of arrival, respectively. The test statistic is derived by first multiplying the received signal by the complex conjugate of the receive antenna steering vector corresponding to the AOA, and then summing over all time and frequency resources:

$$\breve{z} = \sum_{k=0}^{K-1}\sum_{m=0}^{M-1}\mathbf{a}_{\text{rx}}^{H}(\hat{\theta})\tilde{\mathbf{y}}_{k,m} = \tilde{\alpha}\left\|\mathbf{a}_{\text{rx}}(\hat{\theta})\right\|^2\underbrace{\sum_{k=0}^{K-1}\sum_{m=0}^{M-1}\mathbf{a}_{\text{tx}}^{T}(\hat{\theta})\mathbf{f}_k^{(0)}x_m^{(0)}\mathrm{e}^{-j2\pi m\Delta f\tilde{\tau}}}_{=P} + \underbrace{\sum_{k=0}^{K-1}\sum_{m=0}^{M-1}\mathbf{a}_{\text{rx}}^{H}(\hat{\theta})\mathbf{n}_{k,m}}_{=\breve{n}}$$
$$= \tilde{\alpha}NP + \breve{n} \sim \mathcal{CN}\left(\tilde{\alpha}NP, NKM\sigma^2\right),$$

where it is used that $\left\|a_{\text{rx}}(\hat{\theta})\right\|^2 = N$. $\breve{z}$ is then normalized

$$z = \frac{\breve{z}}{\sqrt{\text{var}(\breve{z})/2}} = \frac{\breve{z}}{\sqrt{NMK\sigma^2/2}} \sim \mathcal{CN}\left(\frac{\sqrt{2N}\tilde{\alpha}P}{\sqrt{KM}\sigma}, 2\right).$$

Since z is circular symmetric complex normally distributed $\text{Re}\{z\}^2$ and $\text{Im}\{z\}^2$ are both independent and normally distributed with variances 1. Hence, $|z|^2$ have a non-central χ^2 distribution with 2 degrees of freedom and non-centrality parameter ρ [34, p. 3]:

$$|z|^2 = \text{Re}\{z\}^2 + \text{Im}\{z\}^2 \sim \chi_2^2(\rho).$$

Where the non-centrality parameter ρ is given by [34, p. 3]:

$$\rho = \mathbb{E}[\text{Re}\{z\}]^2 + \mathbb{E}[\text{Im}\{z\}]^2 = |\mathbb{E}[z]|^2 = \frac{2N\left|\tilde{\alpha}\right|^2|P|^2}{KM\sigma^2}.$$

$|z|^2$ will be used as the test statistic. Using this, a p-value for the hypothesis test can be computed. A p-value represents the probability of obtaining a test result at least as extreme as the one observed, under the assumption that the null hypothesis is correct.

The p-value is calculated under the null hypothesis that the strongest possible targets are present.

$$p = \mathbb{P}(|z|^2 > \left|z^{\text{obs}}\right|^2 \,||\alpha_{\max}|^2) = Q_1\left(\sqrt{\rho}, \left|z^{\text{obs}}\right|\right)$$

where Q_1 is the Marcum Q-function, $|\alpha_{\max}|^2$ is the channel gain of the strongest possible target and z^{obs} is the observed signal [34, p. 3]. z^{obs} is calculated in the same manner as z, using the received signal $\mathbf{y}_{k,m}$.

$|\alpha_{\max}|^2$ can be determined either experimentally or by using an upper bound on the radar cross-section $\sigma_{\text{RCS, max}}$ of the targets and the minimum distance $d_{\min}$ a target can be from the radar. This can then be used to calculate the maximum channel gain of a target [35, p. 2817]:

$$|\alpha_{\max}|^2 = \frac{E_s^{(0)}\lambda^2\sigma_{\text{RCS, max}}}{(4\pi)^3 d_{\min}^4}. \tag{3.2}$$

The time of arrival of the theoretical target $\tilde{\tau}$ are given by

$$\tilde{\tau} = \frac{2d_{\min}}{c}. \tag{3.3}$$

The p-values are calculated assuming that the strongest possible target is present, which is the worst-case scenario for distinguishing between no interference and interference. Hence, a lower p-value is a strong indicator that there is no interference [23, pp. 334–335]. Note that in hypothesis testing, one can only reject the null hypothesis; that is, it is only possible to provide evidence against the null hypothesis, not to prove that the alternative hypothesis is true [23, pp. 328–329].

The p-value can be used to reject the null hypothesis by setting a significance level γ, and rejecting the null hypothesis if $p \leq \gamma$. In doing so, the null hypothesis is falsely rejected with probability γ [23, p. 335].

There are four possible outcomes when performing hypothesis testing: True Negative (TN), which occurs when the null hypothesis is not rejected, given that the null hypothesis is true, True Positive (TP), which occurs when the null hypothesis is rejected, and the alternative hypothesis is true, False Positive (FP), when the null hypothesis is rejected but is true; and False Negative (FN) when the null hypothesis is not rejected but the alternative hypothesis is true. This is summarised in the confusion matrix shown in Table 3.1 [30, p. 170].

True State \ Decision	Fail to reject H^0	Reject H^0
H^0 is true	True Negative (TN)	False Positive (FP)
H^1 is true	False Negative (FN)	True Positive (TP)

Table 3.1: Confusion matrix for hypothesis testing.

Performance Metrics

To evaluate the performance of the hypothesis test, the performance metrics True Positive Rate (TPR) and False Positive Rate (FPR) are used.

The FPR is the proportion of rejected null hypotheses out of the total number of true null hypotheses [30, p. 172]

$$FPR = \frac{FP}{FP + TN}.$$

Given that the null hypothesis and the corresponding p-values are rejected at a significance level of γ, it is expected that the FPR will be equal to γ when the null hypothesis is easily fulfilled [23, p. 335].

The TPR is the proportion of correctly rejected null hypotheses out of the total number of true alternative hypotheses [30, p. 172]

$$TPR = \frac{TP}{TP + FN}.$$

3.3 Interfered Subcarrier Detection

In this section, the hypothesis test used for interfered subcarrier detection will be presented, along with the Benjamini-Hochberg procedure, which will be used to control the False Discovery Rate (FDR) of the test.

After determining which path is a LOS path, the subcarriers used by the interferer are detected. To detect which subcarrier m experiences interference, the following hypothesis test is used:

$$H_m^0 : \text{No interference on subcarrier } m$$
$$H_m^1 : \text{LOS interference on subcarrier } m.$$

H_m^0 represents the case when only noise, backscatter from a target, or both is present at subcarrier m. H_m^1 represents the case when subcarrier m contains LOS interference from an interferer. The test is derived similarly to the previous hypothesis test. The main difference is that this test is carried out on individual subcarriers.

The hypothesis test is only carried out on subcarriers that are used by the radar itself, i.e., $m \in \Omega^{(0)}$. This is because it is already known that there is no signal in the unused subcarriers, and hence they are excluded from further processing, meaning that, in total, $N_s = |\Omega^{(i)}|$ tests are made.

It is again assumed that the AOA of path $\hat{\theta}$ has already been estimated. To construct the test statistic, the hypothetical received signal is again multiplied by the complex conjugate of the receive antenna steering vector corresponding to the AOA, and then summed only over time.

$$\begin{aligned}\breve{z}_m = \sum_{k=0}^{K-1} \mathbf{a}_{\mathrm{rx}}^H(\hat{\theta})\tilde{\mathbf{y}}_{k,m} &= \tilde{\alpha}\left\|\mathbf{a}_{\mathrm{rx}}(\hat{\theta})\right\|^2 \underbrace{\sum_{k=0}^{K-1} \mathbf{a}_{\mathrm{tx}}^T(\hat{\theta})\mathbf{f}_k^{(0)} x_m^{(0)} \mathrm{e}^{-j2\pi m\Delta f\tilde{\tau}}}_{=P_m} + \underbrace{\sum_{k=0}^{K-1} \mathbf{a}_{\mathrm{rx}}^H(\hat{\theta})\mathbf{n}_{k,m}}_{=\breve{n}_m} \\ &= \tilde{\alpha}NP_m + \breve{n}_m \sim \mathcal{CN}\left(\tilde{\alpha}NP_m, NK\sigma^2\right).\end{aligned}$$

$\breve{z}_m$ is then normalized

$$z_m = \frac{\breve{z}_m}{\sqrt{\mathrm{var}(\breve{z}_m)/2}} = \frac{\breve{z}_m}{\sqrt{NK\sigma^2/2}} \sim \mathcal{CN}\left(\frac{\sqrt{2N}\tilde{\alpha}P_m}{\sqrt{K}\sigma}, 2\right).$$

Again, $|z_m|^2$ is used as the test statistic, which follows a non-central χ^2 distribution with 2 degrees of freedom and a non-centrality parameter ρ_m, given by [34, p. 3]:

$$\rho_m = \mathbb{E}[\mathrm{Re}\{z_m\}]^2 + \mathbb{E}[\mathrm{Im}\{z_m\}]^2 = |\mathbb{E}[z_m]|^2 = \frac{2N\left|\tilde{\alpha}\right|^2\left|P_m\right|^2}{K\sigma^2}.$$

Using the test statistic, a p-value for the hypothesis test can be stated. The p-value is then calculated in the same manner as the previous hypothesis test.

$$p_m = \mathbb{P}(|z_m|^2 > \left|z_m^{\mathrm{obs}}\right|^2 \,||\alpha_{\max}|^2) = Q_1\left(\sqrt{\rho_m}, \left|z_m^{\mathrm{obs}}\right|\right).$$

The maximum channel gain of the theoretically strongest possible target, $|\alpha_{\max}|^2$ and the hypothetical time of arrival $\tilde{\tau}$ from the target are calculated using (3.2) and (3.3), respectively, in the same manner as in the previous hypothesis test. z_m^{obs} is calculated in the same manner as z_m, using the received signal $\mathbf{y}_{k,m}$.

The p-value can be used to reject H_m^0 by setting a significance level γ, and reject H_m^0 if $p_m \leq \gamma$. However, this introduces a probability of γ for a type-1 error, i.e., rejecting H_m^0 when it is actually true [23, p. 335]. This issue becomes more pronounced as the number of hypothesis tests increases. In the context of interference detection, this is problematic, as it raises the risk of misclassifying non-interfered subcarriers as interfered.

To mitigate this, one can control the probability of making at least one false positive error across all tests, known as the family-wise error rate (FWER). A common method for controlling FWER is the Bonferroni correction, which adjusts the significance level to account for the number of simultaneous tests [10, p. 1953]. However, this increases the likelihood of false negatives. This is problematic because it raises the likelihood of missing interfered subcarriers.

Instead, the proportion of rejected hypotheses that are false positives can be controlled. This can be done using false discovery rate (FDR) control.

False Discovery Rate Control

FDR is the expected value of false discovery proportion (FDP), which is the proportion of false positives to the total number of rejected hypothesis tests. The FDR is given by [3, p. 291]

$$\text{FDR} = \mathbb{E}[FDP] = \mathbb{E}\left[\frac{FP}{\max(1, FP + TP)}\right].$$

The denominator ensures that FDR $= 0$ when $FP + TP = 0$. The FDR can be controlled using the Benjamini-Hochberg procedure [3], which will be presented in the following.

Definition 3.1 (Benjamini-Hochberg procedure)
Let $i \in \{0, \ldots, N_s - 1\}$ denote one of the N_s null hypotheses H_i^0, with the corresponding p-value p_i and let

$$p_{(0)} \leq p_{(1)} \leq \cdots \leq p_{(N_s-1)}$$

denote the order p-values and $H_{(i)}^0$ denotes null the hypothesis corresponding to $p_{(i)}$. Then by letting

$$k = \underset{i}{\text{argmax}}\, p_{(i)} \leq \frac{i}{N_s} q^*.$$

where $q^* \in [0, 1]$ be the significance level, $H_{(i)}^0$ are rejected for $i \in \{0, \ldots, k\}$. [3, p. 293]

Using the Benjamini-Hochberg procedure, FDR can be controlled, which is stated in the following theorem.

Theorem 3.2
By applying the Benjamini-Hochberg procedure on N_s independent p-values, then

$$\text{FDR} \leq \frac{TN + FP}{N_s} q^* \leq q^*.$$

Meaning that the FDR is upper bound by $q*$. [3, Theorem 1]

To detect the interfered subcarriers, p-values will be calculated for each subcarrier used by the radar. It is assumed that the additive noise is independent, and thus the p-values for each subcarrier are independent. Therefore, by using the Benjamini-Hochberg procedure to reject the null hypothesis, it is ensured that FDR $\leq q^*$. This is done for each of the LOS paths, and the union of these interfered subcarriers forms the set of all interfered subcarriers, denoted by $\Omega^{(i)}$.

True Discovery Rate

Another measure of the power is the True Discovery Rate (TDR). It measures the proportion of rejections that are actually true positives.

The TDR is the expected value of the True Discovery Proportion (TDP), which is the proportion of correctly rejected null hypotheses among all rejected hypotheses [12, p. 3]

$$\mathrm{TDR} = \mathbb{E}[\mathrm{TDP}] = \mathbb{E}\left[\frac{TP}{\max(1, TP + FN)}\right].$$

.

3.4 Range Estimation

After identifying the interfered subcarriers, the final step is to estimate the range and corresponding channel gains of both the targets and the interferers.

This is done using only the set of non-interfered subcarriers $\Omega^{(s)} = \Omega^{(0)} \setminus \Omega^{(i)}$ where $\Omega^{(0)}$ denotes the set of subcarriers used by the radar itself. The AOA of the targets has already been estimated in the first step. The range now needs to be estimated for each of them. However, a challenge arises because only a subset of the subcarriers is available for the estimation. A common method for range estimation is to apply the Inverse Discrete Fourier Transform (IDFT) along the subcarriers and find peaks in the spectrogram, or to use subspace methods such as the MUSIC algorithm, which is also used for AOA estimation [4, p. 3]. However, the received signal is not equidistantly sampled, as only a subset of the subcarriers is used. This results in sidelobes in the estimated range, as the signal is no longer continuous. This results in degraded target detection performance and ghost targets, which is undesirable [26, p. 1] [22, p. 143].

To mitigate this, it was proposed in [26] and [22] to use methods from compressed sensing. In compressed sensing, it is assumed that a signal can be represented in a basis using a vector with few non-zero entries [9, pp. 3–4]. Compressed sensing is commonly used in scenarios where the underlying signal is sparsely sampled, for example, in medical imaging [9, pp. 9–12]. Hence, it is suitable here as the received signal is sparse in the subcarrier domain.

In [26], it was proposed to use the Orthogonal Matching Pursuit (OMP) algorithm, which was first proposed in [31]. The OMP algorithm is greedy, meaning that it takes a sequence of locally optimal steps to find a solution. The most optimal step is found by selecting the column of the basis matrix that is most correlated with the current residual. Then, it orthogonalizes by projecting the signal onto the span of the selected basis vectors [31, p. 4656].

To use the OMP algorithm for sensing, a basis must be constructed that consists of the channel responses corresponding to different parameter values [26, p. 2].

The OMP algorithm is executed as many times as there are targets present. However, in the cases considered here, it is assumed that there is only one target per AOA. This means that

the step of projecting the signal onto the span of the selected basis can be skipped, and only the correlation step is needed. Hence, the following presents a method for estimating the time of arrival by finding the delay $\hat{\tau}$ that maximises the correlation between the theoretical channel response and the received signal. This will also be used to calculate the Maximum Likelihood Estimate (MLE) of the channel gain $\hat{\alpha}$.

It is assumed that the interference has been perfectly estimated in the previous steps and only backscattering from the radar's own signal is considered. Hence, only the subcarriers in $\Omega^{(s)}$ are used for the calculation of the estimate of the time of arrival.

To calculate the correlation for different delays, the received signal $\mathbf{y}_{k,m}$ is vectorised by first stacking it across time and then across subcarriers,

$$\mathbf{y} = \left[\mathbf{y}_{1,0}^\top, \dots, \mathbf{y}_{K-1,0}^\top, \mathbf{y}_{0,1}^\top, \dots, \mathbf{y}_{K-1,M-1}^\top\right]^\top.$$

Let $\hat{\theta}$ be one of the estimated AOA of a target or an interferer. Then, the steering vector of the channel, which is also stacked across time and then across subcarriers, is given by:

$$\mathbf{g}(\tau) = \left(\mathbf{b}(\tau) \odot \mathbf{x}^{(0)}\right) \otimes \mathbf{t}^{(0)}(\hat{\theta}) \otimes \mathbf{a}_{\text{rx}}(\hat{\theta}),$$

where $\otimes$ and $\odot$ are the Kronecker product and Hadamard product, respectively and

$$\mathbf{t}^{(0)}(\hat{\theta}) = \begin{bmatrix} \mathbf{a}_{\text{tx}}^\top(\hat{\theta})\mathbf{f}_0^{(0)} \\ \mathbf{a}_{\text{tx}}^\top(\hat{\theta})\mathbf{f}_1^{(0)} \\ \vdots \\ \mathbf{a}_{\text{tx}}^\top(\hat{\theta})\mathbf{f}_{K-1}^{(0)} \end{bmatrix} \in \mathbb{C}^K, \quad \mathbf{x}^{(0)} = \begin{bmatrix} x_0^{(0)} \\ x_1^{(0)} \\ \vdots \\ x_{M-1}^{(0)} \end{bmatrix} \in \mathbb{C}^M, \quad \mathbf{b}(\tau) = \begin{bmatrix} 1 \\ \mathrm{e}^{j2\pi\Delta f\tau} \\ \vdots \\ \mathrm{e}^{j2\pi(M-1)\Delta f\tau} \end{bmatrix} \in \mathbb{C}^M,$$

where $x_m^{(s)}$ is the subcarrier that is not interfered with and is given by

$$x_m^{(s)} = \begin{cases} 1 & \text{if } m \in \Omega^{(s)} \\ 0 & \text{otherwise.} \end{cases}$$

By this, the time of arrival can be estimated by finding the $\hat{\tau}$ for which the received signal $\mathbf{y}$ is most correlated with $\mathbf{g}$, i.e.

$$\hat{\tau} = \underset{\tau}{\text{argmax}} \ \left|\mathbf{g}^H(\tau)\mathbf{y}\right|.$$

Using this, the range of the target can be calculated as

$$\hat{d} = \frac{c\hat{\tau}}{2}.$$

Furthermore, the channel gain can be estimated as [14, p. 1398]

$$\hat{\alpha} = \frac{\mathbf{g}^H(\hat{\tau})\mathbf{y}}{\|\mathbf{g}(\hat{\tau})\|^2}.$$

This is the MLE of the channel gain.

4 Numerical Experiments

In this chapter, numerical experiments are performed to validate the performance of the individual parts of the proposed algorithm.

Only a scenario with a single interferer and a single target is considered in the numerical experiments. It's important to note that only the individual components of the algorithm are validated, not the algorithm as a whole. The individual parts of the algorithm are validated using perfect prior knowledge of the parameters estimated in the previous steps.

First, the normalised transmitted power of the beamformer is presented to validate its performance. Next, the Angle of Arrival (AOA) estimation is validated by calculating the Root Mean Squared Error (RMSE) of the estimated AOA of a target, both with and without interference. Following this, the performance of the Line-of-Sight (LOS) detection is validated by calculating the False Positive Rate (FPR) and the True Positive Rate (TPR) of the hypothesis test. The interfered subcarrier detection is then validated by calculating the True Discovery Proportion (TDP) and False Discovery Proportion (FDP) of the hypothesis test used to detect interfered subcarriers. Lastly, the range estimation is validated by calculating the RMSE of the estimated range to the target, both with and without interference mitigation. This RMSE is then compared to the Cramér-Rao Lower Bound (CRB) of the range.

The hyperparameters common to all numerical experiments are shown in Table 4.1.

Parameter	**Description**	**Value**
f_c	Carrier frequency	77GHz
λ	Wavelength	3.89mm
W	Bandwidth	38.4MHz
N	Number of receive and transmit antennas	4
K	Number of OFDM symbols	25
M	Number of total subcarriers	128
N_s	Number of subcarriers used	64
Δ_f	Subcarrier spacing	300kHz
N_0	Noise power spectral density	-173dBm
σ^2	Noise variance per symbol	$1.24 \cdot 10^{-15}$W
$\sigma_{\text{RCS, target}}$	Target radar cross section	1m^2
$\sigma_{\text{RCS, interfere}}$	Interfere radar cross section	1m^2
$\sigma_{\text{RCS, max}}$	Maximum radar cross section of a target	1m^2
d_{min}	Minimum distance of a target	5m

Table 4.1: Hyperparameters used in the numerical experiments.

The hyperparameters were chosen to mimic what could be used in the automotive industry in the future.

The carrier frequency is set to 77 GHz, which is within the band allocated by the International Telecommunication Union for future automotive mmWave radar sensors [24, p. 60]. Four antennas are used for both transmission and reception. A higher number of antennas could lead to higher AOA resolution, and a higher number of antennas is more common at mmWave frequencies. However, in the automotive industry, a lower number of antennas is more common as high angular resolution is not always needed [24, p. 60].

The bandwidth is fairly large, which results in high range resolution [36, p. 2819]. However, since only a subset of the total available subcarriers is used, some performance might be lost depending on whether the number of used subcarriers is sufficient to accurately estimate the delay [26, pp. 1–2].

Both the target and the interferer have a radar cross-section of 1m^2. Only thermal noise is considered. The noise variance is calculated using the method presented in Section 2.3. It is assumed that the radar operates at $T_{\text{room}} = 295\text{K}$, which is room temperature (22C°) which gave a noise power spectral density of -173dBm.

The total number of subcarriers available is 128, but only half of them, 64, are used at any given time by the radar and the interferer. The two sets of subcarriers used are chosen at random by the radar and the interferer. When only one interferer is present, then the number of interfered subcarriers follows a hypergeometric distribution [22, p. 145][23, p. 121]. If the set of interfered subcarriers is denoted by $\Omega^{(i)}$ then the expected number of interfered subcarriers is:

$$\mathbb{E}[|\Omega^{(i)}|] = \frac{N_s^2}{M} = 32.$$

Meaning that, on average, half of the subcarriers used by the radar experience interference [23, p. 121].

The maximum RCS $\sigma_{\text{RCS, max}}$ of a hypothetical target is set equal to that of the target 1m^2. This is done to validate that the target paths are misclassified as a LOS path when the target is closer than $d_{\min} = 5\text{m}$.

In the following, the Signal-to-Noise Ratio (SNR) will be defined as the ratio of the gain of the scattered path to the target, $|\alpha^{\text{sctr}}|^2$, to the variance of the noise

$$\text{SNR} = \frac{|\alpha^{\text{sctr}}|^2}{\sigma^2}.$$

Likewise, the Interference-to-Noise Ratio (INR) will be defined as the ratio of the gain of the LOS path between the interferer and the radar $|\alpha^{\text{LOS}}|^2$ to the variance of the noise

$$\text{INR} = \frac{|\alpha^{\text{LOS}}|^2}{\sigma^2}.$$

The transmit power of the radar and the interferer is set so that the SNR or INR equals a predefined set value at a given distance.

4.1 Beamforming

This section demonstrates the performance of the beamformer presented in Section 2.4. The beamforming of a radar has a significant impact on its performance. Therefore, before performing the numerical experiments, the normalised transmitted power of the beamformer that both the radar and the interferer are shown in Figure 4.1.

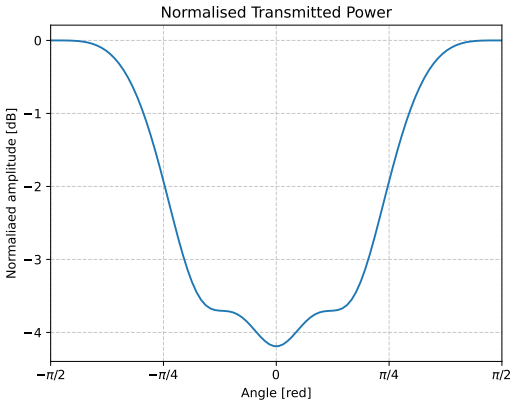

Figure 4.1: The normalised transmitted power of both the radar and the interferer.

It can be seen that the beamforming is not uniform. There is a large dip in power directly in front of the radar. It drops down to under $-4\,\text{dB}$, which means that the power is more than halved at that angle. However, the power is more uniformly distributed in the angular ranges of $[-\frac{\pi}{2}, -\frac{\pi}{4}]$ and $[\frac{\pi}{4}, \frac{\pi}{2}]$. This will impact the performance of the estimation of both AOA and the range of targets placed directly in front of the radar.

4.2 Angle of Arrival Estimation

In the following, the AOA estimation is validated, which was presented in Section 3.1. As an error measure, the Root Mean Squared Error (RMSE) of the estimated AOA of the target is used. This is estimated as

$$\text{RMSE}_\theta = \sqrt{\frac{1}{T}\sum_{t=0}^{T-1}(\theta_{\text{target}} - \hat{\theta}_t)^2}.$$

Where T is the number of trials, θ_{target} is the true AOA of the target, and $\hat{\theta}_t$ is the t-th estimate of the AOA.

Two scenarios are considered: In the first scenario, only the target is present, i.e no interference. Hence, only the backscatter path of the target is simulated. The target is placed with an AOA to radar of $\theta_{\text{target}} = \frac{\pi}{3}$ $(60°)$ and at a distance to the from the radar of $10\,\text{m}$. In this scenario, it is assumed that it is known that only one target is present, so the dimensionality of the noise subspace D is set to one. The AOA estimation is performed by finding the maximum of the MUSIC spectrum.

In the second scenario, an interferer is also present at an $\theta_{\text{interfere}} = -\frac{\pi}{3}$ $(-60°)$ and also at a distance form the radar of 10 m. The transmitted power of the interferer is set such that the INR is 10 dB. In the second scenario, the dimensionality of the noise subspace D is set to 2, as there are now two AOAs. The target's AOA is estimated by finding the two highest peaks in the MUSIC spectrum and assigning the largest angle as the AOA of the target.

The RMSE of the AOA of the target is shown in Figure 4.2 for both the scenario with no interference and the scenario with interference.

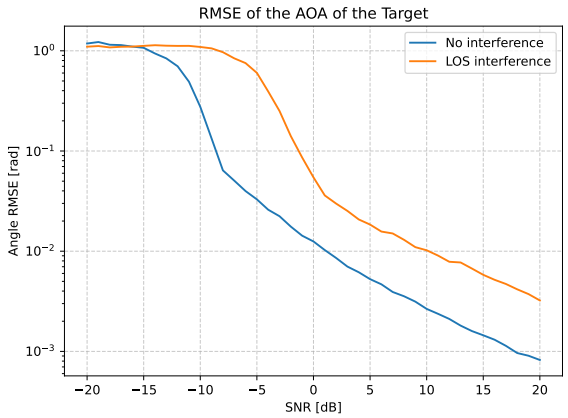

Figure 4.2: The RMSE of the estimated AOA of a target is evaluated both with and without an interferer present. The target is positioned at a distance of 10m from the radar and with an AOA of $\frac{\pi}{3}$. The interferer is positioned at a distance of 10 m and with an AOA of $-\frac{\pi}{3}$ and INR = 10dB.

Generally, AOA estimation performs better with no interference at all SNRs. It can be seen that the RMSE increases rapidly around an SNR of −9 dB for the case with no interference and at 0 dB with interference. At higher SNRs, the performance improves exponentially with SNR, which is expected. However, at SNRs higher than 0 dB, the performance is degraded by around 10 dB when the interferer is present.

The reason for the degraded performance when the interferer is present is that the LOS path AOA is much stronger than the AOA from the target because the path gain is higher. This is illustrated in Figure 4.3, which shows the MUSIC spectrum with no interferer present at SNR = 5 dB and SNR = −5 dB, and with the interferer present at the same SNRs and INR = 10 dB.

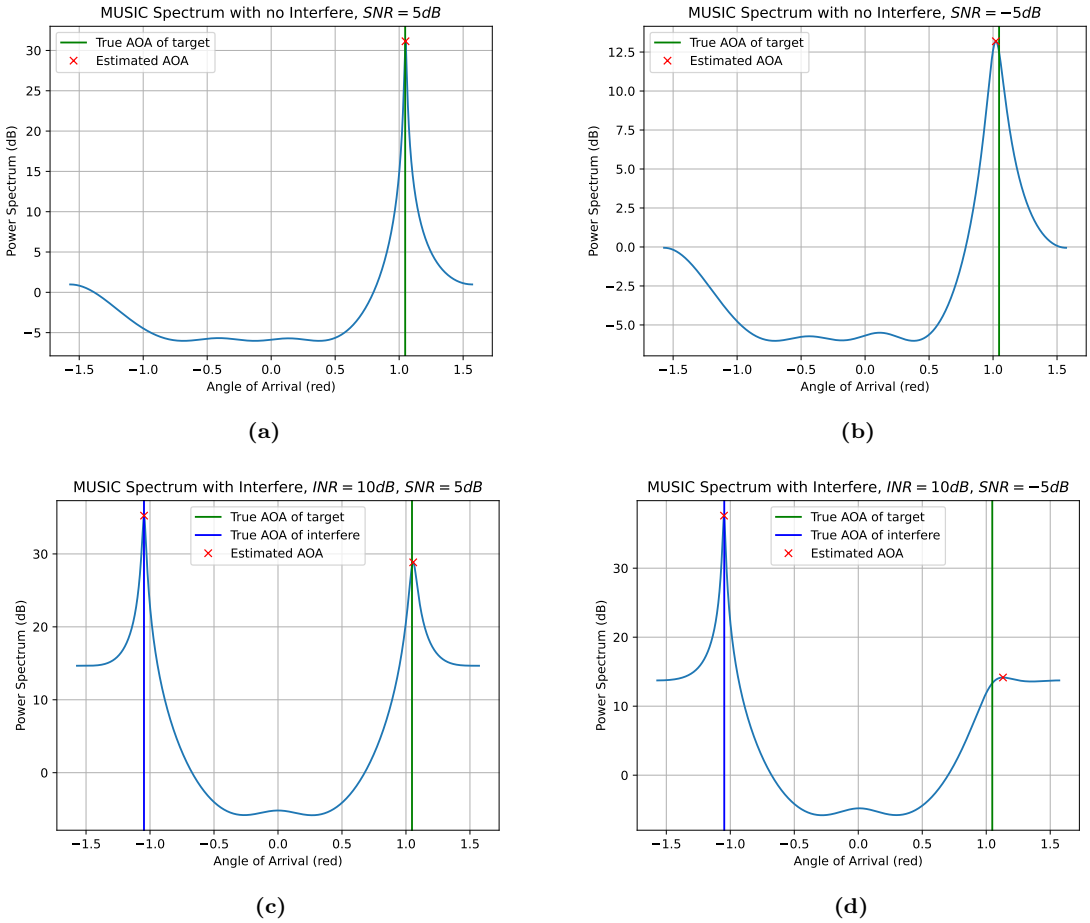

Figure 4.3: The MUSIC spectrum in dB for a range of scenarios: a stronger target (SNR = 5 dB) and a weaker target (SNR = −5 dB), both with and without interference with INR = 10dB.

It can be seen in Figure 4.3a and Figure 4.3b that the MUSIC spectrum has stronger peaks at the AOA of the target when no interferer is present, where the SNR is 5 dB and −5 dB, respectively.

In Figure 4.3c, it can be seen that the MUSIC spectrum has strong peaks at both the AOA of the target and the interferer when a strong target with an SNR = 5 dB is present. However, as shown in Figure 4.3d, when a weaker target with an SNR = −5 dB is present, the interference drowns out the peak from the target, which leads to worse estimation performance compared to when no interference is present.

4.3 Line-of-Sight Detection

In this section, the hypothesis test presented in Section 3.2, which is used to detect the LOS path, are validated. The hypothesis tests in this section are evaluated with perfect prior knowledge of the AOAs of the interferer and the target. The null hypothesis is rejected at a significance level of $\gamma = 0.1$.

First, the FPR (False Positive Rate) and the TPR (True Positive Rate) are calculated as a function of position relative to the radar. This is done by simulating 100 realisations with only a target at the given position with an RCS of $\sigma_{\text{target}} = 1\,\text{m}^2$, which corresponds to the null hypothesis being true. Then, 100 realisations with an interferer at the given location, which corresponds to the alternative hypothesis being true, are simulated. From these 200 trials, the FPR and TPR are calculated.

The transmit power of the radar is set so that the SNR of a target at 10 m is equal to 20 dB. The transmit power of the interferer is set to be the same as that of the radar. The FPR and TPR as a function of position can be seen on Figure 4.4.

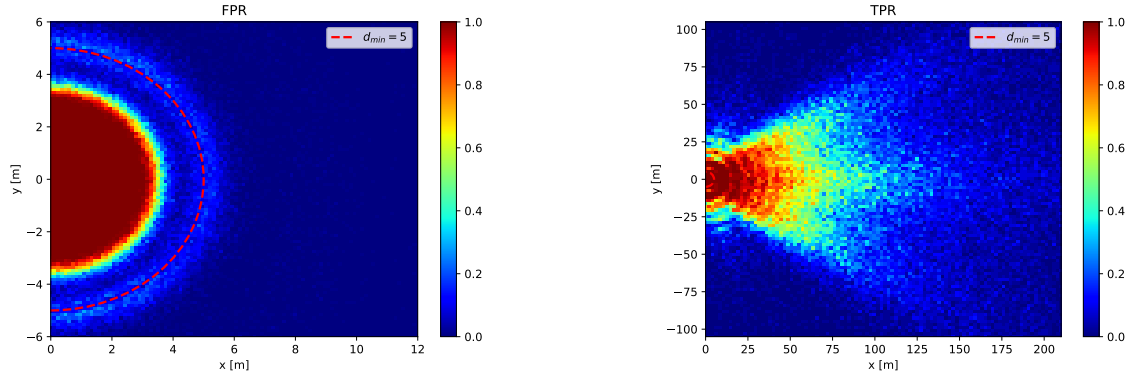

(a) **(b)**

Figure 4.4: The FPR and TPR as functions of position, computed over 100 trials with the target present at the position and 100 trials with the interferer at the same position.

The TPR is the probability of misclassifying a LOS path as a target path. The TPR as a function of position can be seen on Figure 4.4b. It can be seen that the LOS path is always correctly classified up to a distance of 14 m. The TPR is higher in front of the radar. This is due to the beamformer used. When less energy is transmitted in a direction, less energy is expected to be reflected back. Hence, an interferer with a weaker LOS path (and thus at a greater distance) can be detected. To the sides where the transmitted power is higher, the detection distance is smaller. The ripple in the TPR is due to the fact that the phase shift from the time of arrival is not compensated for. This introduces a phase shift in the received signal as a function of distance, which can be seen as ripples in the figures.

The FPR is the probability of classifying a target path as an LOS path. The FPR can be seen as a function of position on Figure 4.4a. When the target is closer than $d_{\text{min}} = 5\,\text{m}$, the target should be misclassified as an interferer, meaning that the FPR should be 1. However, in Figure 4.4a, it can be seen that the FPR is one when the target is closer than 4 m to the radar, and that between 4 m and 5 m, the target is still classified as a target. This is again due to the delay of the received signal not being compensated for.

When the target is around 5 m from the radar, the FPR rises again to 0.1, which is the significance level. This is because at this distance, the null hypothesis is exactly true, meaning

that it should be rejected at the given significance level. This can also be seen in Figure 4.5, which shows the FPR at a constant distance of 5 m from the radar as a function of AOA. It can be seen that the FPR is controlled at the significance level of 0.1, which is what is expected.

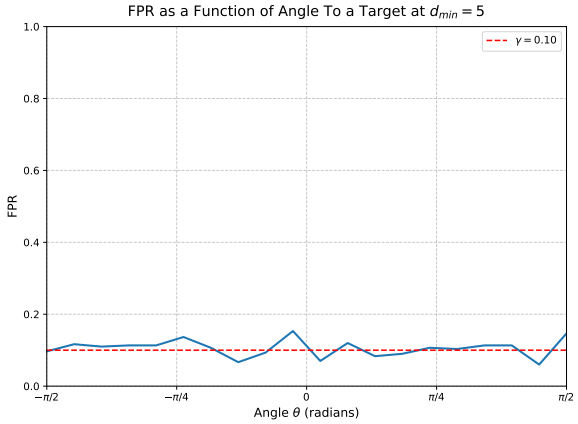

Figure 4.5: The FPR as a function of angle is evaluated, given a target at a constant distance of $d_{\min} = 5$m from the radar.

On Figure 4.6 TPR is shown with a target at a distance of 10m from the radar with an AOA of $\frac{\pi}{3}$. The INR is adjusted by increasing the transmitted power of the interferer.

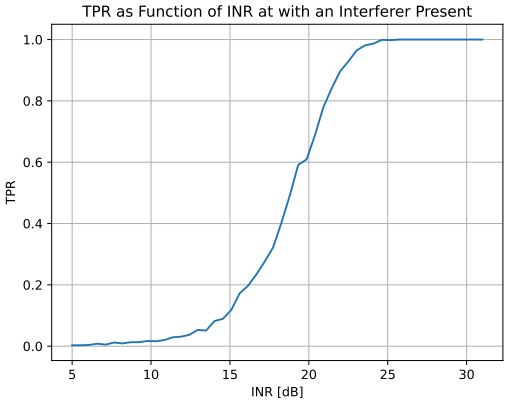

Figure 4.6: The TPR as a function INR where the interferer is 10m form the radar at a AOA of $\frac{\pi}{3}$.

It can be seen that at an AOA of $\frac{\pi}{3}$, the interferer is almost always detected when the INR is higher than 25 dB. However, the TPR rises slowly as a function of INR.

This is due to the fact that the received energy is calculated by summing over all subcarriers, including those not used by the radar itself. This introduces more noise, which leads to more uncertainty in the statistical test.

4.4 Interfered Subcarrier Detection

Next, the hypothesis test that is used to detect interfering subcarriers, presented in Section 3.3, is validated. Again, the tests are performed with perfect prior knowledge of the AOA of both the target and the interferer. The hypothesis tests are rejected using the Benjamini-Hochberg procedure with a significance level of $q^* = 0.10$.

The hypothesis test is validated by calculating the True Discovery Proportion (TDP) and False Discovery Proportion (FDP) for 20 realisations and then taking the ensemble average over them to get an estimate of the True Discovery Rate (TDR) and False Discovery Rate (FDR), respectively. In Figure 4.7a, the TDR are shown as a function of location when an interferer is present at the given location. In Figure 4.7b, the FDR is shown as a function of the location of a target.

The transmit power of the radar and the interferer is set in the same manner as in the previous section.

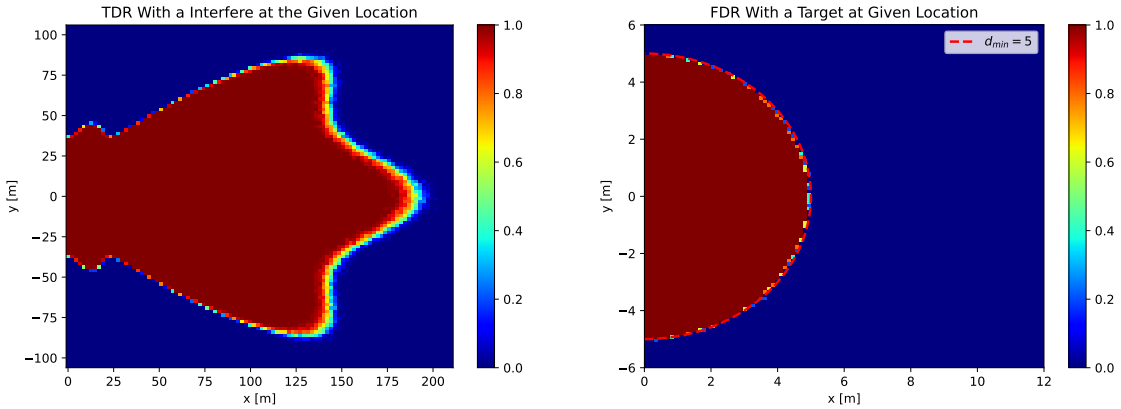

(a) **(b)**

Figure 4.7: The TDR with an interferer present at the given location is shown in **(a)**. The FDR are shown in **(b)** with a target at the given location.

The TDR is the probability of correctly identifying an interfering subcarrier, given that the subcarrier is interfered. When the interferer is present, on average, half of the subcarriers are affected by interference. In Figure 4.7a, it can be seen that the interfered subcarriers can be detected correctly in front of the radar out to a distance of 175 m. However, to the sides of the radar, it can only correctly detect the interfered subcarriers out to a distance of 25 m. This is due to the non-uniform beamforming. In the directions with less transmitted power, less power is expected to be reflected back by a hypothetical target. Hence, a weaker interferer is needed to exceed the detection threshold and be detected. So, the performance of the detection is a function of the radar's beamforming.

FDR is the probability of incorrectly identifying a non-interfered subcarrier as being interfered with. In Figure 4.7b, the FDR is shown as a function of the location of a target. It can be

seen that the FDR is 1 when the target is closer than the minimum distance to the radar, meaning that the backscatter from the target is misclassified as interference. This is expected as the channel gain is larger than $|\alpha^{\max}|^2$. The FDR is zero outside the minimum distance, which means that backscatter from a target is never misclassified as being interference.

In Figure 4.8, the FDR with a target at a constant distance of 5 m, which is $d_{\min}$, is shown as a function of AOA.

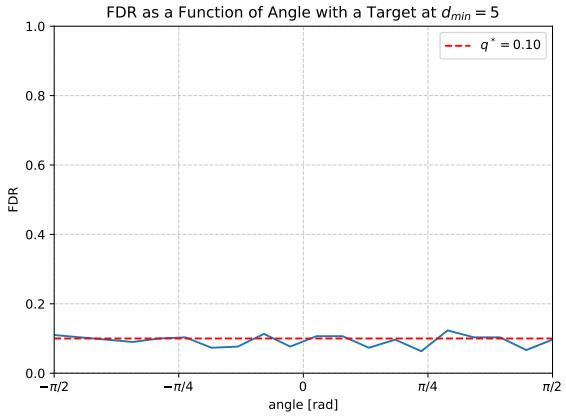

Figure 4.8: The FDR with a target present at a distance of $d_{\min} = 5$ m is shown as a function of angle to the target.

At $d_{\min}$, the null hypothesis is exactly true. As the hypotheses are rejected using the Benjamini-Hochberg procedure according to Theorem 3.2, the FDR should be less than or equal to q^*, which is also observed in Figure 4.8.

On Figure 4.9 the TDR is shown as a function with an interferer present at an angle of $\frac{\pi}{3}$ and at a distance of 10m.

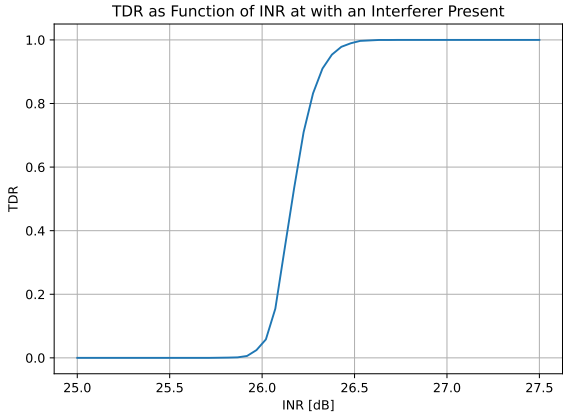

Figure 4.9: TDR as a function of INR with an interferer present at an angle of $\frac{\pi}{3}$ and at a distance of 10m.

It can be seen that the TDR is 1 when the INR is larger than 26.5 dB.

4.5 Range Estimate

In this section, the range estimation is validated, which was presented in Section 3.4. Again, the tests are performed with perfect prior knowledge of the Angle of Arrival (AOA) for both the target and the interferer. It's also assumed that the AOAs are correctly classified as either LOS or target paths, and that the subcarriers used by the interferer are correctly identified.

As a performance metric, the RMSE of the estimated distance, which is given by:

$$\mathrm{RMSE}_d = \sqrt{\mathbb{E}\left[(d_{\mathrm{target}} - \hat{d})^2\right]},$$

where d_{target} is the true distance to the target, and $\hat{d}$ is the estimate of the distance to the target. If it is assumed that the estimator is unbiased, then the RMSE of the estimator can be lower-bounded by the square root of the Cramér-Rao Lower Bound (CRB) [20, p. 12]

$$\mathrm{RMSE}_d \geq \sqrt{\mathrm{CRB}_d}.$$

The CRB for distance estimation in an OFDM radar has been derived in [4, pp. 34–35] and is given by:

$$\mathrm{CRB}_d = \frac{3c}{\mathrm{SNR} 8\pi^2 K M (M^2 - 1)\Delta f^2}.$$

This lower bound is derived under the assumption that all subcarriers are used for estimation. This means that it is a conservative lower bound, as at most half of the subcarriers are used in the simulation. Therefore, the square root of the CRB will be used as a benchmark for the RMSE of the distance.

By replacing the expectation with the ensemble average, the RMSE can be estimated as:

$$\widehat{\mathrm{RMSE}}_d = \sqrt{\frac{1}{T}\sum_{t=0}^{T-1}(d_{\mathrm{target}} - \hat{d}_t)^2},$$

where T is the number of trials and $\hat{d}_t$ is the t-th estimate of the distance to the target.

On Figure 4.10, the RMSE of the range as a function of SNR is shown for three scenarios: Only the target is present (no interference), represented by the blue line. The interferer is present, but all subcarriers are used for range estimation (no interference mitigation), represented by the yellow line. The interferer is present, and only the non-interfered subcarriers are used for range estimation (with interference mitigation), represented by the green line. Together with the square root of the CRB, the red line. The interferer transmit power is set to have an INR of 10 dB.

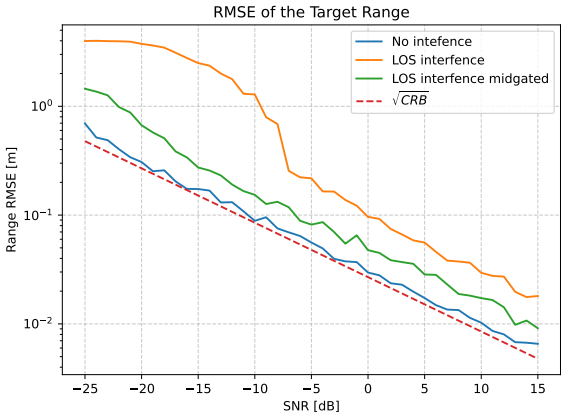

Figure 4.10: RMSE of the estimated distance to the target as a function of SNR. This figure compares three scenarios: without interference, with interference but no mitigation, and with interference mitigation. These results are presented alongside the square root of the CRB as a benchmark. The target is placed at an angle of $\frac{\pi}{3}$ to the radar, and the interferer is also at an angle of $-\frac{\pi}{3}$. Both are at a distance of 10 m, and the INR is 10 dB.

It can be seen that with no interference, the range can be estimated to almost the CRB. This demonstrates that even when using only half of the subcarriers, the performance is only slightly degraded.

When interference is present, the range estimation performance degrades by approximately 10 dB. Without mitigation, it's not possible to estimate the range of a target with a weaker signal than −8 dB.

By employing interference mitigation, the performance significantly improves by 5-7 dB compared to having no interference mitigation. Consequently, the performance is only degraded by 4-5 dB when compared to the ideal scenario with no interference at all.

5 Discussion

In this thesis, an algorithm has been proposed to mitigate interference in OFDM radar systems. A channel model was developed to simulate an environment where an interferer uses the same resources as the radar. An OFDM scheme was proposed where only a random subset of subcarriers is used for sensing. This enables the radar to sense when interferers are present, as only a subset of the subcarriers are interfered. An algorithm was proposed to do sensing when interference is present. The algorithm estimates the subcarriers used by the interferers using the LOS path. The non-interfered subcarriers and then used to do sensing. First, the number of paths and angle of arrival (AOA) are estimated using the MUSIC algorithm. Then, a hypothesis test was proposed to determine which paths are LOS paths. Another hypothesis was then proposed to identify the subcarriers used by the interferers using the LOS paths. Then, the range and channel gain of each target are estimated by only using the non-interfered subcarriers.

The beamformer is constructed by dividing the angular interval $\left[-\frac{\pi}{2}, \frac{\pi}{2}\right]$ into 25 evenly spaced beams switching at each OFDM symbol. This is a simple beamformer which is used to show the principle of the algorithm. It has a weakness, having a -4dB drop in power at 0 rad's as shown on Figure 4.1. A more suitable beamformer with more uniform power distribution may lead to better performance.

The chosen modulation scheme is OFDM, which was originally developed for communication purposes. Using a waveform like FMCW, which is specifically designed for sensing, can lead to better sensing performance. However, OFDM is very flexible as it can be used for integrated sensing and communication, which can save on hardware cost. More relevant to this project, OFDM can also be adapted to utilise frequency resources by employing only a subset of the available subcarriers. Hence, the reduction in sensing performance is justified, as interference mitigation is also possible.

The subcarriers used in this project were randomly chosen, but a more advanced scheme could be advantageous. For instance, only the interfered subcarriers can be changed from one OFDM frame to the next. If it is assumed that both the interferer and the radar can reliably estimate the interfered subcarriers, it ensures that the sensing performance in the current OFDM frame is at least as good as that of the previous one. This is because it's guaranteed that subcarriers not experiencing interference in the last frame will remain uninterfered with in the next frame. This is under the assumption that a new interferer does not appear between the two frames.

The individual parts of the proposed algorithms were implemented and numerically verified.

The AOA estimation algorithm can estimate AOA of a target even in the presence of an interferer. Figure 4.2 shows that AOA of a target can be estimated with a precision of 0.1 rad with SNR = 0dB and INR = 10dB. At SNR lower than 0dB, the target is overpowered

by the interferer as indicated on Figure 4.3, and AOA can not be estimated reliably.

To identify which AOA stems from a LOS path, a hypothesis test is used. If the received energy is larger than the biggest hypothetical backscattered energy, it is assumed to be a LOS path. The hypothesis test was able to identify the LOS path with an INR of 25 dB.

The test statistic is calculated by summing over all subcarriers, also those not used by the radar itself. The benefit is that it could be easier to detect an interferer that uses multiple subcarriers not used by the radar. This way, an interferer can be identified, and this information can be used for other purposes, like establishing a communication link. The drawback of summing over all subcarriers is a higher noise floor, leading to a degraded SNR. In general, a higher SNR will make a better-performing hypothesis test. This could be mitigated by only summing over the subcarriers used by the radar itself. This will make it harder to detect an interferer if it is only using a few overlapping subcarriers with the radar itself.

Furthermore, the test statistic used for LOS detection changes with the time of arrival, which leads to the ripples observed in Figure 4.4b. This could be mitigated by using a different test statistic that considers the absolute values of each received subcarrier at each OFDM symbol before summing them. This approach would make the test statistic independent of the time of arrival.

Another hypothesis test was employed to identify the subcarriers experiencing interference. This test was able to identify the interfered subcarriers down to an INR of 26.5 dB. It performs better than the LOS hypothesis test because it operates on individual subcarriers, as there is no phase distortion from the time of arrival. This can be seen in Figure 4.7a, where the ripples observed in Figure 4.4b are not present.

The proposed range estimator is based on correlation. Generally, the range estimator with LOS interference mitigation can obtain the same performance at a 5-7dB lower SNR. More importantly, it is capable of estimating targets at low SNR's below -5dB, which is not possible without interference mitigation.

6 Conclusion

Radars play a crucial role in driver assistance in automotive systems. The likelihood of interference increases as the deployment of radars goes up, if they use the same allocated frequency bands. To ensure adequate performance, interference mitigation techniques need to be developed. This leads to the following problem statement:

How can a hypothesis test be developed to detect interference in an OFDM mmWave radar system, and can sensing performance be improved by avoiding the use of detected interfered resources?

First, an OFDM schema was introduced, which could mitigate interference by using only a random subset of subcarriers. Then, a channel model was developed, modelling a scenario where a radar senses the environment in the presence of interferers.

An algorithm was proposed that can sense in the presence of interference. This is done by first estimating the number of paths and their Angle Of Arrival (AOA) using the MUSIC algorithm. Next, a hypothesis test is used to determine which paths are Line Of Sight (LOS) paths from an interferer and which are backscattered signals from targets. Then another hypothesis test is used on the LOS paths to determine which subcarriers contain interference. The range and path gain of the target are estimated using the non-interfered subcarriers. The individual parts of the algorithm have been validated in numerical experiments.

The AOA can be estimated with interference of INR = 10dB down to target SNR = 0dB. The LOS hypothesis test can correctly classify a LOS path with INR down to 25dB given a perfect prior of the AOA. The hypothesis test to classify interference in a subcarrier always classifies non-interfered subcarriers correctly. It classifies all the interfered subcarriers to down INR = 26.5dB.

The range can be estimated reliably with interference mitigation using perfect a priori knowledge of the AOA of the target. Without interference mitigation, this has 7dB worse performance for the same root mean square error and is not possible below SNR = -5dB.

Two hypothesis tests have been constructed. One hypothesis test to determine LOS paths and one hypothesis test to determine interfered subcarriers. Using a priori AOA, the range of the target can be estimated by doing interference mitigation. The algorithms have not been implemented as a complete system, so it can not be concluded whether total sensing performance has been improved.

7 Further Work

The complete system should be implemented in order to test in full if total sensing performance has been improved.

The test statistic used for LOS detection could be reworked so that it doesn't depend on the time of arrival. This might lead to better performance.

The beamformer should be redesigned for more uniform power distribution. This way, the effect of the beamformer will be minimised on the performance of the system.

Bibliography

[1] Zohair Abu-Shaban et al. "Error Bounds for Uplink and Downlink 3D Localization in 5G Millimeter Wave Systems". In: *IEEE Transactions on Wireless Communications* 17.8 (Aug. 2018). Conference Name: IEEE Transactions on Wireless Communications, pp. 4939–4954. ISSN: 1558-2248. DOI: 10.1109/TWC.2018.2832134. URL: https://ieeexplore.ieee.org/document/8356190/?arnumber=8356190 (visited on 02/14/2025).

[2] Ofer Bar-Shalom et al. "Accurate Time Synchronization for Automotive Cooperative Radar (CoRD) Applications". In: *2020 IEEE International Radar Conference (RADAR)*. ISSN: 2640-7736. Apr. 2020, pp. 500–505. DOI: 10.1109/RADAR42522.2020.9114861. URL: https://ieeexplore.ieee.org/document/9114861 (visited on 04/15/2025).

[3] Yoav Benjamini and Yosef Hochberg. "Controlling the False Discovery Rate: A Practical and Powerful Approach to Multiple Testing". In: *Journal of the Royal Statistical Society. Series B (Methodological)* 57.1 (1995). Publisher: [Royal Statistical Society, Oxford University Press], pp. 289–300. ISSN: 0035-9246. URL: https://www.jstor.org/stable/2346101 (visited on 03/20/2025).

[4] Klaus Martin Braun. *OFDM Radar Algorithms in Mobile Communication Networks*. de. ISSN: 1433-3821. 2014. DOI: 10.5445/IR/1000038892. URL: https://publikationen.bibliothek.kit.edu/1000038892 (visited on 02/12/2025).

[5] J. Capon. "High-resolution frequency-wavenumber spectrum analysis". In: *Proceedings of the IEEE* 57.8 (Aug. 1969). Conference Name: Proceedings of the IEEE, pp. 1408–1418. ISSN: 1558-2256. DOI: 10.1109/PROC.1969.7278. URL: https://ieeexplore.ieee.org/document/1449208/?arnumber=1449208 (visited on 05/01/2025).

[6] Gisela K. Carvajal et al. "Comparison of Automotive FMCW and OFDM Radar Under Interference". In: *2020 IEEE Radar Conference (RadarConf20)*. ISSN: 2375-5318. Sept. 2020, pp. 1–6. DOI: 10.1109/RadarConf2043947.2020.9266449. URL: https://ieeexplore.ieee.org/document/9266449/?arnumber=9266449 (visited on 04/21/2025).

[7] Xiang Cheng et al. "Integrated Sensing and Communications (ISAC) for Vehicular Communication Networks (VCN)". In: *IEEE Internet of Things Journal* 9.23 (Dec. 2022). Conference Name: IEEE Internet of Things Journal, pp. 23441–23451. ISSN: 2327-4662. DOI: 10.1109/JIOT.2022.3191386. URL: https://ieeexplore.ieee.org/document/9830717/?arnumber=9830717 (visited on 04/21/2025).

[8] Juergen Dickmann et al. ""Automotive radar the key technology for autonomous driving: From detection and ranging to environmental understanding"". In: *2016 IEEE Radar Conference (RadarConf)*. ISSN: 2375-5318. May 2016, pp. 1–6. DOI: 10.1109/RADAR.2016.7485214. URL: https://ieeexplore.ieee.org/document/7485214 (visited on 03/03/2025).

[9] Simon Foucart and Holger Rauhut. *A Mathematical Introduction to Compressive Sensing*. en. Applied and Numerical Harmonic Analysis. New York, NY: Springer, 2013. ISBN: 978-0-8176-4948-7. DOI: 10.1007/978-0-8176-4948-7. URL: https://link.springer.com/10.1007/978-0-8176-4948-7 (visited on 09/20/2024).

[10] Jelle J. Goeman and Aldo Solari. "Multiple hypothesis testing in genomics". en. In: *Statistics in Medicine* 33.11 (2014). _eprint: https://onlinelibrary.wiley.com/doi/pdf/10.1002/sim.6082, pp. 1946–1978. ISSN: 1097-0258. DOI: 10.1002/sim.6082. URL: https://onlinelibrary.wiley.com/doi/abs/10.1002/sim.6082 (visited on 05/12/2025).

[11] Jürgen Hasch et al. "Millimeter-Wave Technology for Automotive Radar Sensors in the 77 GHz Frequency Band". In: *IEEE Transactions on Microwave Theory and Techniques* 60.3 (Mar. 2012). Conference Name: IEEE Transactions on Microwave Theory and Techniques, pp. 845–860. ISSN: 1557-9670. DOI: 10.1109/TMTT.2011.2178427. URL: https://ieeexplore.ieee.org/document/6127923/?arnumber=6127923 (visited on 04/10/2025).

[12] Jianliang He, Bowen Gang, and Luella Fu. *False Discovery Control in Multiple Testing: A Brief Overview of Theories and Methodologies*. arXiv:2411.10647 [stat] version: 1. Nov. 2024. DOI: 10.48550/arXiv.2411.10647. URL: http://arxiv.org/abs/2411.10647 (visited on 04/29/2025).

[13] Musa Furkan Keskin, Henk Wymeersch, and Visa Koivunen. *ICI-Aware Parameter Estimation for MIMO-OFDM Radar via APES Spatial Filtering*. arXiv:2102.06756 [eess]. Feb. 2021. DOI: 10.48550/arXiv.2102.06756. URL: http://arxiv.org/abs/2102.06756 (visited on 02/07/2025).

[14] Musa Furkan Keskin, Henk Wymeersch, and Visa Koivunen. "MIMO-OFDM Joint Radar-Communications: Is ICI Friend or Foe?" In: *IEEE Journal of Selected Topics in Signal Processing* 15.6 (Nov. 2021). Conference Name: IEEE Journal of Selected Topics in Signal Processing, pp. 1393–1408. ISSN: 1941-0484. DOI: 10.1109/JSTSP.2021.3109431. URL: https://ieeexplore.ieee.org/document/9529026/?arnumber=9529026&tag=1 (visited on 02/21/2025).

[15] Hyowon Kim et al. "RIS-Aided Monostatic Sensing and Object Detection with Single and Double Bounce Multipath". In: *2023 IEEE International Conference on Communications Workshops (ICC Workshops)*. ISSN: 2694-2941. May 2023, pp. 1883–1889. DOI: 10.1109/ICCWorkshops57953.2023.10283494. URL: https://ieeexplore.ieee.org/document/10283494/?arnumber=10283494&tag=1 (visited on 02/18/2025).

[16] Visa Koivunen et al. "Multicarrier ISAC: Advances in waveform design, signal processing, and learning under nonidealities". In: *IEEE Signal Processing Magazine* 41.5 (Sept. 2024). Conference Name: IEEE Signal Processing Magazine, pp. 17–30. ISSN: 1558-0792. DOI: 10.1109/MSP.2024.3420492. URL: https://ieeexplore.ieee.org/document/10770016 (visited on 03/08/2025).

[17] H. Krim and M. Viberg. "Two decades of array signal processing research: the parametric approach". In: *IEEE Signal Processing Magazine* 13.4 (July 1996), pp. 67–94. ISSN: 1558-0792. DOI: 10.1109/79.526899. URL: https://ieeexplore.ieee.org/document/526899/ (visited on 05/14/2025).

[18] Yu-Chien Lin et al. "Non-Cooperative Interference Avoidance in Automotive OFDM Radars". In: *2019 IEEE 89th Vehicular Technology Conference (VTC2019-Spring)*. ISSN: 2577-2465. Apr. 2019, pp. 1–5. DOI: 10.1109/VTCSpring.2019.8746354. URL: https://ieeexplore.ieee.org/document/8746354/?arnumber=8746354 (visited on 02/21/2025).

[19] Fan Liu et al. "Integrated Sensing and Communications: Toward Dual-Functional Wireless Networks for 6G and Beyond". In: *IEEE Journal on Selected Areas in Communications* 40.6 (June 2022). Conference Name: IEEE Journal on Selected Areas in Communications, pp. 1728–1767. ISSN: 1558-0008. DOI: 10.1109/JSAC.2022.3156632. URL: https://ieeexplore.ieee.org/document/9737357/?arnumber=9737357 (visited on 04/10/2025).

[20] Henrik Madsen and Poul Thyregod. *Introduction to general and generalized linear models*. Texts in statistical science. CRC Press, 2011. ISBN: 978-1-4200-9155-7.

[21] Benjamin Nuss, Leen Sit, and Thomas Zwick. "A novel technique for interference mitigation in OFDM radar using compressed sensing". In: *2017 IEEE MTT-S International Conference on Microwaves for Intelligent Mobility (ICMIM)*. Mar. 2017, pp. 143–146. DOI: 10.1109/ICMIM.2017.7918877. URL: https://ieeexplore.ieee.org/document/7918877/?arnumber=7918877 (visited on 01/23/2025).

[22] Benjamin Nuss and Thomas Zwick. "A novel interference mitigation technique for MIMO OFDM radar using compressed sensing". In: *2017 European Radar Conference (EURAD)*. Oct. 2017, pp. 98–101. DOI: 10.23919/EURAD.2017.8249156. URL: https://ieeexplore.ieee.org/document/8249156/?arnumber=8249156 (visited on 02/10/2025).

[23] Peter Olofsson and Mikael Andersson. *Probability, Statistics, and Stochastic Processes*. English. 2nd edition. Hoboken, N.J: Wiley, May 2012. ISBN: 978-0-470-88974-9.

[24] Fabian Roos et al. "Radar Sensors for Autonomous Driving: Modulation Schemes and Interference Mitigation". In: *IEEE Microwave Magazine* 20.9 (Sept. 2019). Conference Name: IEEE Microwave Magazine, pp. 58–72. ISSN: 1557-9581. DOI: 10.1109/MMM.2019.2922120. URL: https://ieeexplore.ieee.org/document/8792451/?arnumber=8792451 (visited on 02/04/2025).

[25] R. Schmidt. "Multiple emitter location and signal parameter estimation". In: *IEEE Transactions on Antennas and Propagation* 34.3 (Mar. 1986). Conference Name: IEEE Transactions on Antennas and Propagation, pp. 276–280. ISSN: 1558-2221. DOI: 10.1109/TAP.1986.1143830. URL: https://ieeexplore.ieee.org/abstract/document/1143830 (visited on 01/27/2025).

[26] Syed Najaf Haider Shah et al. *Newtonized Orthogonal Matching Pursuit for High-Resolution Target Detection in Sparse OFDM ISAC Systems*. arXiv:2411.03191 [eess]. Nov. 2024. DOI: 10.48550/arXiv.2411.03191. URL: http://arxiv.org/abs/2411.03191 (visited on 02/04/2025).

[27] Merrill Skolnik. *Introduction to Radar Systems*. English. Boston, Mass. Burr Ridge, IL Dubuque, IA: McGraw-Hill Education, 2001. ISBN: 978-0-07-288138-7.

[28] John D. Storey. "A direct approach to false discovery rates". en. In: *Journal of the Royal Statistical Society: Series B (Statistical Methodology)* 64.3 (2002). _eprint: https://onlinelibrary.wiley.com/doi/pdf/10.1111/1467-9868.00346, pp. 479–498. ISSN: 1467-9868. DOI: 10.1111/1467-9868.00346. URL: https://onlinelibrary.wiley.com/doi/abs/10.1111/1467-9868.00346 (visited on 04/09/2025).

[29] Christian Sturm et al. "Spectrally interleaved multi-carrier signals for radar network applications and multi-input multi-output radar". en. In: *IET Radar, Sonar & Navigation* 7.3 (2013). _eprint: https://onlinelibrary.wiley.com/doi/pdf/10.1049/iet-rsn.2012.0040, pp. 261–269. ISSN: 1751-8792. DOI: 10.1049/iet-rsn.2012.0040. URL: https://onlinelibrary.wiley.com/doi/abs/10.1049/iet-rsn.2012.0040 (visited on 01/29/2025).

[30] Alaa Tharwat. "Classification assessment methods". In: *Applied Computing and Informatics* 17.1 (Jan. 2021). Publisher: Emerald Publishing Limited, pp. 168–192. ISSN: 2634-1964, 2210-8327. DOI: 10.1016/j.aci.2018.08.003. URL: https://doi.org/10.1016/j.aci.2018.08.003 (visited on 04/28/2025).

[31] Joel A. Tropp and Anna C. Gilbert. "Signal Recovery From Random Measurements Via Orthogonal Matching Pursuit". In: *IEEE Transactions on Information Theory* 53.12 (Dec. 2007), pp. 4655–4666. ISSN: 1557-9654. DOI: 10.1109/TIT.2007.909108. URL: https://ieeexplore.ieee.org/document/4385788/ (visited on 05/05/2025).

[32] Christian Waldschmidt, Juergen Hasch, and Wolfgang Menzel. "Automotive Radar — From First Efforts to Future Systems". In: *IEEE Journal of Microwaves* 1.1 (Jan. 2021). Conference Name: IEEE Journal of Microwaves, pp. 135–148. ISSN: 2692-8388. DOI: 10.1109/JMW.2020.3033616. URL: https://ieeexplore.ieee.org/document/9318758/?arnumber=9318758 (visited on 02/04/2025).

[33] Xinhai Wang et al. "Method to suppress narrowband interference for OFDM radar". In: *The Journal of Engineering* 2019.21 (Nov. 2019). Publisher: The Institution of Engineering and Technology, pp. 8170–8174. DOI: 10.1049/joe.2019.0751. URL: https://digital-library.theiet.org/doi/10.1049/joe.2019.0751 (visited on 02/13/2025).

[34] Henk Wymeersch and Gonzalo Seco-Granados. "Adaptive Detection Probability for mmWave 5G SLAM". In: *2020 2nd 6G Wireless Summit (6G SUMMIT)*. Mar. 2020, pp. 1–5. DOI: 10.1109/6GSUMMIT49458.2020.9083898. URL: https://ieeexplore.ieee.org/document/9083898 (visited on 01/18/2025).

[35] Henk Wymeersch and Gonzalo Seco-Granados. “Radio Localization and Sensing—Part I: Fundamentals”. In: *IEEE Communications Letters* 26.12 (Dec. 2022). Conference Name: IEEE Communications Letters, pp. 2816–2820. ISSN: 1558-2558. DOI: 10.1109/LCOMM.2022.3206821. URL: https://ieeexplore.ieee.org/document/9893187/?arnumber=9893187 (visited on 01/23/2025).

[36] Henk Wymeersch and Gonzalo Seco-Granados. “Radio Localization and Sensing—Part II: State-of-the-Art and Challenges”. In: *IEEE Communications Letters* 26.12 (Dec. 2022). Conference Name: IEEE Communications Letters, pp. 2821–2825. ISSN: 1558-2558. DOI: 10.1109/LCOMM.2022.3206846. URL: https://ieeexplore.ieee.org/document/9893114/?arnumber=9893114 (visited on 01/23/2025).

[37] Henk Wymeersch et al. “5G mmWave Positioning for Vehicular Networks”. In: *IEEE Wireless Communications* 24.6 (Dec. 2017). Conference Name: IEEE Wireless Communications, pp. 80–86. ISSN: 1558-0687. DOI: 10.1109/MWC.2017.1600374. URL: https://ieeexplore.ieee.org/document/8246850/?arnumber=8246850 (visited on 04/14/2025).

[38] H.C. Yildirim et al. “Impact of Interference on OFDM based Radars”. In: *2020 IEEE 91st Vehicular Technology Conference (VTC2020-Spring)*. ISSN: 2577-2465. May 2020, pp. 1–5. DOI: 10.1109/VTC2020-Spring48590.2020.9128852. URL: https://ieeexplore.ieee.org/document/9128852/?arnumber=9128852 (visited on 04/10/2025).